

# A NUMERICAL STUDY OF THE TSUNAMI RESPONSE OF THE HAWAIIAN ISLANDS

By  
EDDIE N. BERNARD

MAY 1976

HAWAII INSTITUTE OF GEOPHYSICS  
UNIVERSITY OF HAWAII, HONOLULU  
and  
JOINT TSUNAMI RESEARCH EFFORT  
PACIFIC MARINE ENVIRONMENTAL LABORATORY  
ENVIRONMENTAL RESEARCH LABORATORY, NOAA

**HAWAII INSTITUTE OF GEOPHYSICS**  
UNIVERSITY OF HAWAII





A NUMERICAL STUDY OF THE TSUNAMI  
RESPONSE OF THE HAWAIIAN ISLANDS\*

By

Eddie N. Bernard


May 1976

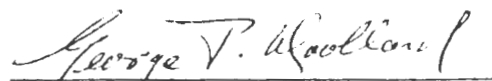
Hawaii Institute of Geophysics  
University of Hawaii, Honolulu

and

Joint Tsunami Research Effort  
Pacific Marine Environmental Laboratory  
Environmental Research Laboratories, NOAA

\*A DISSERTATION SUBMITTED TO THE GRADUATE DIVISION OF TEXAS A&M  
UNIVERSITY IN PARTIAL FULFILLMENT OF THE REQUIREMENTS FOR THE  
DEGREE OF DOCTOR OF PHILOSOPHY IN OCEANOGRAPHY, AUGUST 1976.

  
\_\_\_\_\_  
Director  
Joint Tsunami Research Effort

  
\_\_\_\_\_  
Director  
Hawaii Institute of Geophysics



## ABSTRACT

*The response of linearized long waves to the eight major Hawaiian Islands is investigated numerically using a mathematical model of the island system. A spline interpolation scheme is utilized to convert the actual soundings of the island bathymetry to a 5.5 km square grid closely approximating the topography of the islands. A time-marching, central difference, explicit scheme is used to evaluate the wave field by the linear, long wave, Eulerian equations of motion and continuity in Cartesian coordinates for a frictionless, homogeneous fluid. The condition of no normal flow is employed at the island shorelines and a localized interpolation technique is utilized at the outer boundary to simulate a free-flow boundary. Verification of the numerical procedure is accomplished by agreement with analytic solutions of steady-state problems involving wave interaction with geometric islands in both constant and variable depth cases.*

*Island response is determined by using a generalized time sequence input with a stipulated spectrum in the tsunami frequency range. This input is time-stepped through the model for a duration sufficient to establish a statistical equilibrium within the system. The shoreline hydrographs, which record the time history of water elevation around the islands, are Fourier analyzed to obtain spectra for each shoreline point. These spectra are divided by the input spectrum to obtain transfer functions which represent the relative response of the system to waves in the tsunami period range. Verification of the response analysis is judged in terms of the agreement with the analytic response of a variable depth geometric island to a set of tsunami period waves. A technique for determining the period cut off of a particular model system is demonstrated by comparison of responses of the same model using coarse and fine grids.*

*The response analysis methods are applied to the model of the Hawaiian Islands for the case of a tsunami originating in the Alaskan region. Transfer functions are shown in averaged and contoured form for the island system and each individual island. The model study reveals that the numerical technique is appropriate for the response study of the Hawaiian Islands, that there are at least nine characteristic periods in the tsunami range to which the islands respond, and that interinsular reflections generate areas of high energy concentrations.*



## ACKNOWLEDGMENTS

To Shirley Bernard, my wife, I give thanks for the understanding, patience, and support required to complete this degree.

To Professor Robert O. Reid, Drs. Andrew C. Vastano and Gaylord R. Miller, who have given much of their time and many of their ideas toward this research, I extend grateful appreciation. Discussions with members of the Joint Tsunami Research Effort in Honolulu, Hawaii and with Drs. Davis Fahlquist and William Bryant of Texas A&M University have also been helpful during the course of this study.

This research was sponsored by the Joint Tsunami Research Effort and by the National Science Foundation through the National Center for Atmospheric Research. The computer graphics contained in this report were accomplished through the assistance of Tom Reid.





## TABLE OF CONTENTS

| Chapter    |   | Page |
|------------|---|------|
| I          | INTRODUCTION . . . . .                                | 1    |
|            | 1.1 <u>General Discussion</u> . . . . .               | 1    |
|            | 1.2 <u>Objectives</u> . . . . .                       | 5    |
| II         | THE MATHEMATICAL MODEL IN CARTESIAN COORDINATES .     | 7    |
|            | 2.1 <u>The Equations of Motion and Continuity</u> . . | 7    |
|            | 2.2 <u>Numerical Analogue in Cartesian Grid</u>       |      |
|            | <u>System</u> . . . . .                               | 8    |
|            | 2.3 <u>Lateral Boundary Conditions</u> . . . . .      | 12   |
|            | 2.4 <u>Confirmation of the Numerical Procedure</u> .  | 19   |
| III        | APPLICATION OF THE MODEL FOR RESPONSE ANALYSIS .      | 31   |
|            | 3.1 <u>Generalized Time Sequence Input</u> . . . . .  | 31   |
|            | 3.2 <u>Verification of the Response Technique</u> .   | 32   |
| IV         | A STUDY OF THE RESPONSE OF THE HAWAIIAN ISLANDS       |      |
|            | TO A TSUNAMI APPROACHING FROM ALASKA . . . . .        | 39   |
|            | 4.1 <u>The Hawaiian Islands Numerical Model</u> . . . | 39   |
|            | 4.2 <u>Results of the Hawaiian Islands Response</u>   |      |
|            | <u>To Generalized Input Approaching from</u>          |      |
|            | <u>Alaska</u> . . . . .                               | 41   |
| V          | SUMMARY AND RECOMMENDATIONS . . . . .                 | 70   |
|            | 5.1 <u>Summary of Results</u> . . . . .               | 70   |
|            | 5.2 <u>Future Research</u> . . . . .                  | 71   |
| REFERENCES | . . . . .   | 72   |

## LIST OF TABLES

| Table  | Page |
|--|------|
| 2.1. Parameters of verification comparison for the<br>cylindrical island . . . . .   | 23   |
| 2.2. Parameters of verification comparison for the<br>parabolic island . . . . .     | 28   |
| 4.1. Values of averaged energy ratio peaks from<br>individual islands . . . . .      | 54   |
| 4.2. Travel times between islands and around<br>islands at selected depths . . . . . | 66   |

# LIST OF FIGURES

| Figure   | Page |
|--|------|
| 1.1. Runups around Kauai for the April 1, 1946 tsunami. . . . .  | 4    |
| 2.1. Grid arrangement for explicit, space-staggered scheme. . . . .  | 11   |
| 2.2. Reflecting boundary condition. . . . .  | 14   |
| 2.3. The open boundary condition is graphically represented by the time scale (upper part) and the spatial scale (lower part). . . . .   | 17   |
| 2.4. Boundary configuration with one-dimensional reference canal. . . . .  | 20   |
| 2.5. Cylindrical island of radius $r_0$ in constant depth ocean $H_0$ . . . . .  | 23   |
| 2.6. Cartesian coordinate approximation of a cylindrical island where, for example, the value of $\theta$ at $A = 86.5^\circ$ , $B = 22.5^\circ$ , $C = -22.5^\circ$ , and $D = -86.5^\circ$ . . . . . | 24   |
| 2.7. Comparison of numerical model of cylindrical island with analytic solution for a 4-minute incident wave period. The incident side of the island is $180^\circ$ . . . . .                          | 25   |
| 2.8. As in Fig. 2.7 except for 8-minute incident wave period. . . . .  | 26   |
| 2.9. Parabolic island of radius $r_0$ with variable topography out to $r_1$ . . . . .  | 28   |
| 2.10. Comparison of numerical model of parabolic island with analytic solution for an 8 minute incident wave period. The incident side of the island is $180^\circ$ . . . . .                          | 29   |
| 3.1. Comparison of numerical and analytic transfer functions (upper part) for the parabolic island of Fig. 2.9 and comparison of numerical and analytic input spectra (lower part). . . . .            | 34   |

| Figure |   | Page |
|--------|---|------|
| 3.2.   | Comparison of coarse numerical and analytic transfer functions (upper part) for the parabolic island of Fig. 2.9 and comparison of numerical and analytic input spectra (lower part). . . . . | 37   |
| 4.1.   | Hawaiian Islands model showing topographic area with surrounding constant depth region. . . . .   | 40   |
| 4.2.   | Perspective view of the Hawaiian model topography looking from the southeast. Each grid point represents nine grid points of the actual model. . . . .  | 42   |
| 4.3.   | Comparison of numerical and analytic input spectra for the Hawaiian model. . . . .  | 43   |
| 4.4.   | Average of all shoreline transfer functions of the Hawaiian model for a tsunami originating in the Alaska region. . . . .   | 45   |
| 4.5.   | Average of transfer functions around Niihau. . . . .  | 46   |
| 4.6.   | As in Fig. 4.5 except around Kauai. . . . .   | 47   |
| 4.7.   | As in Fig. 4.5 except around Oahu. . . . .  | 48   |
| 4.8.   | As in Fig. 4.5 except around Molokai. . . . .   | 49   |
| 4.9.   | As in Fig. 4.5 except around Lanai. . . . .   | 50   |
| 4.10.  | As in Fig. 4.5 except around Kahoolawe. . . . .   | 51   |
| 4.11.  | As in Fig. 4.5 except around Maui. . . . .  | 52   |
| 4.12.  | As in Fig. 4.5 except around Hawaii. . . . .  | 53   |
| 4.13.  | Contour of $\sqrt{\text{energy ratio}}$ around Niihau. . . . .  | 56   |
| 4.14.  | As in Fig. 4.13 except for Kauai. . . . .   | 57   |
| 4.15.  | As in Fig. 4.13 except for Oahu. . . . .  | 58   |
| 4.16.  | As in Fig. 4.13 except for Molokai. . . . .   | 59   |
| 4.17.  | As in Fig. 4.13 except for Lanai. . . . .   | 60   |
| 4.18.  | As in Fig. 4.13 except for Kahoolawe. . . . .   | 61   |

| Figure   | Page |
|--|------|
| 4.19. As in Fig. 4.13 except for Maui. . . . .                                       | 62   |
| 4.20. As in Fig. 4.13 except for Hawaii. . . . .                                     | 63   |
| 4.21. Key for grid points around island for seven<br>model Hawaiian Islands. . . . . | 64   |
| 4.22. Key for grid points around the model island<br>of Hawaii. . . . .              | 65   |



# A NUMERICAL STUDY OF THE TSUNAMI RESPONSE OF THE HAWAIIAN ISLANDS

by

Eddie N. Bernard

## CHAPTER I INTRODUCTION

### 1.1 General Discussion

Tsunami is the scientifically accepted term to describe surface gravity waves generated by an oceanic crustal disturbance. The primary sources of these waves are shallow focus (less than 50 km) under-water earthquakes of magnitude 6.5 or greater on the Richter scale. However, not all earthquakes of this type create tsunamis, indicating a strong dependence on the individual generating mechanism and local crustal structure. Once the tsunami is formed, waves radiate in all directions across the ocean from the source. The deep water characteristics of these waves have not been observed, but by theoretical and wave record analyses, it has been deduced that the spectrum of wave periods ranges from 4 to 90 minutes and the deep water wave amplitudes are several meters. The wavelengths of the waves are related to the characteristic length of the seismic source and range from 10 to 100 km. The ratio of depth of water to wavelength indicates that tsunamis are shallow water waves that traverse the ocean basin at a speed proportional to the square root of the depth of water. For example, a wave traveling over a depth of 4000 m has a speed of 713 km per hour. As the waves rapidly spread over the ocean basins they encounter islands and island groups that respond to the

periodicity, amplitude, and approach angle of the waves. In the Pacific Ocean, when an earthquake generates a tsunami in the Aleutian Islands, waves are felt in the southern portion of the Hawaiian Archipelago 4.5 hours later. The present effort concentrates on the response of the major inhabited Hawaiian Islands to remotely generated tsunamis.

Past studies of tsunamis interacting with islands have involved the use of analytic, numerical, and hydraulic models in attempts to understand the complex phenomenon. These models have been employed to simulate the interaction of tsunamis with a single island of simple geometry (Omer and Hall, 1949; Homma, 1950) or with a single island of more complicated geometry and realistic bathymetric data (Jordaan and Adams, 1968; Vastano and Reid, 1970; Brandsma, Divoky, and Hwang, 1974). Verification of the numerical models has been accomplished by analytic and hydraulic comparisons. Further, the approximate agreement between such models and wave record studies is convincing and indicates that numerical models serve as an effective means of studying the interaction phenomenon.

As a tsunami approaches the shorelines of islands, the wave train energy becomes concentrated in a smaller volume of water. The concentration of energy results in larger amplitude waves that become steeper until their advance is arrested in the shoreline region and their energy is partly dissipated along the coast and partly scattered back to sea. While the single island studies have made progress in the understanding of refraction, diffraction, and reflection in the presence of bathymetry which can produce a partial trapping of wave



energy (Longuet-Higgins, 1967), they do not address the problem of the effect of reflection from other islands within an island system. The reflected energy from other islands is superimposed on the locally reflected and trapped waves as well as the incident tsunami and can generate sequences of positive and negative wave interference.

Tsunami reflection by continental shelves has been investigated analytically by Cochrane and Arthur (1948) and applied to the tsunami of April 1, 1946. Shepard *et al.* (1950) believed that reflections within the Hawaiian Islands explained the direction of approach of some of the waves during that tsunami. Unusually high waves from the 1946 tsunami were observed on Kauai at coastal areas opposite Niihau and Oahu (Fig. 1.1). In Fig. 1.1 the peak opposite Oahu represents three observations as reported by Shepard *et al.* (1950). A close examination of the Kauai coastline reveals that the 12.2-m observation at the Oahu azimuth is at the head of a small bay. This localized concentration of energy could account for such a high runup. However, the 7.6- and 9.8-m observations are on a straight coastline with no topographic focusing by the nearshore bathymetry and hence localized concentration of energy does not explain the large amplitudes. The coincidence of larger amplitudes opposite these islands suggests the need for investigation of the reflection of tsunamis within the island system.

A study of a three-island system, which modeled a portion of the Hawaiian Islands, illustrated the local reflection concept (Vastano and Bernard, 1973). This model was of very simple geometric configuration utilizing a polar coordinate system. Since the polar grid

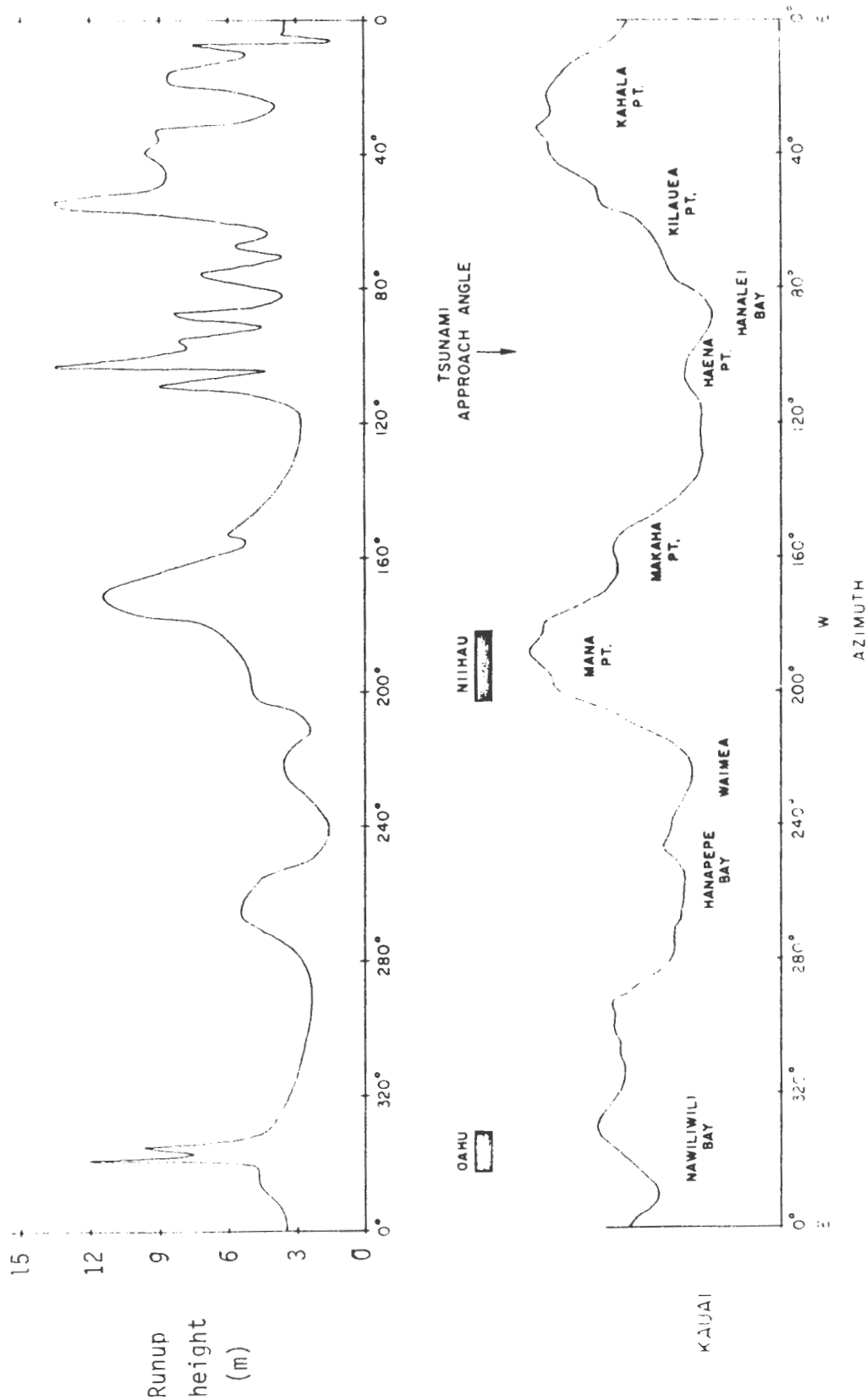


FIG.1.1. Runups around Kauai for the April 1, 1946 tsunami. The upper part shows runup heights while the lower part shows corresponding geographical points around Kauai. The 0° azimuth is the easternmost part of Kauai.

design enabled fine resolution at the center of the model and decreasing resolution with radial distance, only one island could be studied in detail by this coordinate system. To simulate a more realistic model of the Hawaiian Islands, a model employing a rectangular coordinate system was required to permit equal resolution of the model region and to allow multiple islands to be studied simultaneously. This system, utilized in a computer such as a CDC 7600, can adequately and economically simulate tsunami interaction with a topographic model of the Hawaiian Islands.

## 1.2 Objectives

The analytic evaluation of the spectral response for wave-island interaction is feasible only for islands of simple geometric configuration. In view of this limitation, the present study emphasizes the numerical approach to the problem of the response of frequency-limited pulses with island systems of general shapes and general bathymetry, within the framework of linear, undamped, nondispersive long wave theory. To this end the following general objectives are pursued: (1) the development of a numerical model in Cartesian coordinates of long wave interaction with the Hawaiian Islands using charted bathymetric data of the major island system, (2) evaluation of response patterns produced at each island to a specified input representing a generalized time sequence with a known band limited spectrum, corresponding to the tsunami frequency range and originating in the North Pacific, and (3) analysis of the relative tsunami energy distribution at each major island as a function of frequency and

relative position to the other islands.

Within these guidelines the first goal is the confirmation of the numerical modeling technique by agreement with analytic solutions of waves interacting with islands of simple geometry. On verification, investigation of the response of the Hawaiian Islands system can be made. It is to be emphasized that possible dissipation of energy by either bottom friction or nonlinear bore phenomena in the nearshore zone is not considered in this study, implying that the spectral response is generally overestimated.

## CHAPTER II

### THE MATHEMATICAL MODEL IN CARTESIAN COORDINATES

#### 2.1 The Equations of Motion and Continuity

Data gathered at recording stations show tsunamis to be long, small amplitude waves having most of their energy in a band of periods from 4 to 90 minutes. This is a simplified description but adequate for the study of responses for multiple islands. The upper period limit of tsunamis is small enough to allow the effect of the rotation of the earth to be neglected, and the lower limit is still large enough to allow shallow water wave theory to be applied. The approximations of shallow water wave theory require that the vertical component of acceleration is negligible compared to the acceleration of gravity  $g$ . This implies that the vertical distribution of pressure is hydrostatic. Additionally, the horizontal fluid velocities  $(u, v)$  are assumed small compared with the wave speed, and the free surface elevation  $\eta$  is considered small compared to the depth  $H$ . These assumptions permit squares and cross products of these quantities and their derivatives to be smaller in comparison with the linear terms. Further, it is assumed that the fluid is frictionless, homogeneous, irrotational, and incompressible.

Applying these limitations to the Navier-Stokes equations and imposing kinematic boundary conditions at the surface and bottom, the resulting classical, linear, long wave equations of motion and continuity in Cartesian coordinates are :

$$\frac{\partial u}{\partial t} = -g \frac{\partial \eta}{\partial x} \quad (2.1)$$

$$\frac{\partial v}{\partial t} = -g \frac{\partial \eta}{\partial y} \quad (2.2)$$

$$\frac{\partial \eta}{\partial t} = -\frac{\partial(Hu)}{\partial x} - \frac{\partial(Hv)}{\partial y} \quad (2.3)$$

The approximation used in the derivation of these equations will undoubtedly lead to errors in their application to the response study. The size of errors may be estimated nearshore, where the greatest inaccuracy of the wave speed  $\sqrt{gH}$  takes place. Nearshore, the speed is more accurately described by  $\sqrt{g(H+\eta)}$ , where the amplitude is an appreciable part of the depth of water. The numerical model of the Hawaiian Islands takes 50 m as the shallowest depth; therefore, for  $\eta = 5$  m the wave speed will be in error by 5% when only  $\sqrt{gH}$  is used. The shallowest depth in the Hawaiian Island model was chosen to eliminate having the wave amplitude a considerable portion of the water depth and to describe the major bathymetric features of the region. The wave speed can also be incorrect for periods < 5 minutes, since vertical acceleration is of consequence for such periods. For example, the wave speed for a 3-minute period in 4000-m depth is about 8% less than the value given by  $\sqrt{gH}$ . The effect of this error will arise in the phase relationship calculated for shorter period waves around the shorelines of the islands.

## 2.2 Numerical Analogue in Cartesian Grid System

The finite difference representation of a boundary value problem is restricted in resolution by the discrete grid system that models

the continuum, while the minimum grid size is dictated by the available storage capacity of the computer system for a given total area to be modeled. Within this limitation, the primary consideration is an accurate modeling of the waves. Since the rectangular grid evenly divides the area to be modeled, the grid size dictates the shortest period wave that can be described. In the case of monochromatic waves, at least four grid points are needed to define a wave unambiguously. However, the higher the resolution, the less area can be modeled per computer storage space. In order to describe a given area adequately, the limiting factor for the description of waves of low periods is the computer storage and available machine time, since the time step must be compatible with grid size for numerical stability.

The stability criterion for explicit central differences of hyperbolic equations can be stated for a rectangular grid (Platzman, 1958) as

$$(\Delta t \sqrt{gH_{\max}})^2 \leq \frac{1}{\left(\frac{1}{\Delta x}\right)^2 + \left(\frac{1}{\Delta y}\right)^2} \quad (2.4)$$

where  $\Delta x$  and  $\Delta y$  are grid spacings in the x and y directions,  $\Delta t$  is the time increment, and  $H_{\max}$  is the greatest depth in the system. If  $\Delta x = \Delta y$ , one can simplify (2.4) to

$$\Delta t \leq \frac{\Delta x}{\sqrt{2gH_{\max}}} \quad (2.5)$$

For the case of (2.5),  $\Delta t$  is chosen such that the fastest wave

cannot propagate more than one-half of the diagonal of one cell to insure numerical stability.

The finite difference analogue of (2.1), (2.2), and (2.3) is an explicit, space-staggered scheme (Platzman, 1958; Reid and Bodine, 1968; Loomis, 1972). The variables computed are water level,  $\eta$ , from the undisturbed state, and the velocity components  $u$  and  $v$  in the  $x$ - $y$  directions. The velocity grid points are interlaced in space with the water level grid points such that the water level brackets the  $v$  component in the  $y$  direction and the  $u$  component in the  $x$  direction. Fig. 2.1 illustrates the grid arrangement for computation. Let

$$u \{ (i-\frac{1}{2})\Delta x, j \Delta y, n \Delta t \} = u_{i,j}^n \quad (2.6)$$

$$v \{ i \Delta x, (j-\frac{1}{2})\Delta y, n \Delta t \} = v_{i,j}^n \quad (2.7)$$

$$\eta \{ i \Delta x, j \Delta y, (n-\frac{1}{2})\Delta t \} = \eta_{i,j}^n \quad (2.8)$$

where  $i$ ,  $j$ , and  $n$  are integers. The centered difference numerical analogues of (2.3), (2.1), and (2.2), respectively, are

$$\begin{aligned} \eta_{i,j}^{n+1} = & \eta_{i,j}^n - \frac{\Delta t}{\Delta x} \left( H_{i+1,j} u_{i+1,j}^n - H_{i,j} u_{i,j}^n \right) \\ & - \frac{\Delta t}{\Delta y} \left( H_{i,j+1} v_{i,j+1}^n - H_{i,j} v_{i,j}^n \right) \end{aligned} \quad (2.9)$$

$$u_{i,j}^{n+1} = u_{i,j}^n - \frac{g\Delta t}{\Delta x} \left( \eta_{i,j}^{n+1} - \eta_{i-1,j}^{n+1} \right) \quad (2.10)$$



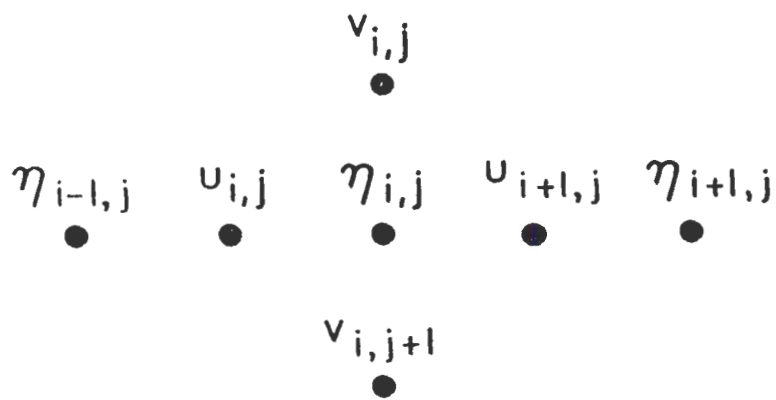


FIG. 2.1. Grid arrangement for explicit, space-staggered scheme.

$$v_{i,j}^{n+1} = v_{i,j}^n - \frac{g\Delta t}{\Delta y} \left( \eta_{i,j}^{n+1} - \eta_{i,j-1}^{n+1} \right) . \quad (2.11)$$

The wave amplitudes at time  $(t_0 + \frac{\Delta t}{2})$  are evaluated using amplitudes at  $(t_0 - \frac{\Delta t}{2})$  and velocities at  $t_0$ ; then the velocities at  $(t_0 + \Delta t)$  are evaluated using velocities at  $t_0$  and wave amplitudes at  $t_0 + \frac{\Delta t}{2}$ . Thus by assigning  $\eta$  at  $t_0 - \frac{\Delta t}{2}$  and  $u, v$  at  $t_0$ , the time marching procedure is calculated:

$$\eta \frac{\Delta t}{2}, u\Delta t, v\Delta t, \eta \frac{3\Delta t}{2}, u(2\Delta t), v(2\Delta t), \dots$$

Because the  $u$  and  $v$  grid points are offset from the grid points, (2.9) reveals that water depths  $H$  are the actual water depths at the positions of  $u$  and  $v$ . To calculate the  $u$  and  $v$  velocities one must usually supply two depth-field arrays to obtain the greatest accuracy for the model. The drawback to such an arrangement is that extra computer storage is required to handle the two arrays. An economical compromise is to set the  $H$  field the same for  $u$  and  $v$ .

### 2.3 Lateral Boundary Conditions

Equations (2.1), (2.2), (2.3) represent free, undamped, gravity waves propagating in a laterally infinite ocean. With only a finite amount of area to model, it is necessary to restrict the bounds of the ocean and to approximate the actual island boundaries in some manner. The Hawaiian Islands were modeled using a reflecting boundary that allows no fluid to pass through an impermeable wall and an open or transparent boundary that allows disturbances to flow through as if

no material boundary existed.

At the shorelines, the Islands are considered to extend vertically through the sea surface as solid, impermeable barriers that totally reflect the impinging waves. This requires a condition of no normal flow, or in terms of wave amplitude

$$\frac{\partial \eta}{\partial n} = 0 . \quad (2.12)$$

The condition on  $\eta$  is selected in order to provide  $\eta$  values on the boundary and because the proper rendition of the condition is facilitated for oblique boundaries as discussed below. Since islands form closed curves of general shape, an appropriate inner boundary condition should allow reflection from a boundary which is at an angle with respect to the grid configuration. To approximate this condition a second order series expansion is utilized to approximate the water elevation in the neighborhood of the boundary by

$$\eta = a_0 + a_1x + a_2y + a_3x^2 + a_4xy + a_5y^2 \quad (2.13)$$

where  $x, y$  are now local coordinates. By taking the derivative of  $\eta$  with respect to its normal, one gets

$$\frac{d\eta}{dn} = (a_1 + 2a_3x + a_4y) \frac{dx}{dn} + (a_2 + a_4x + 2a_5y) \frac{dy}{dn} , \quad (2.14)$$

$\frac{dx}{dn} = \cos \theta$  and  $\frac{dy}{dn} = \sin \theta$  where  $\theta$  is a specified orientation angle characterizing a given point on the island boundary (Fig. 2.2).

The restriction (2.12) requires that

$$(a_1 + 2a_3x + a_4y) \cos \theta + (a_2 + a_4x + 2a_5y) \sin \theta = 0 .$$

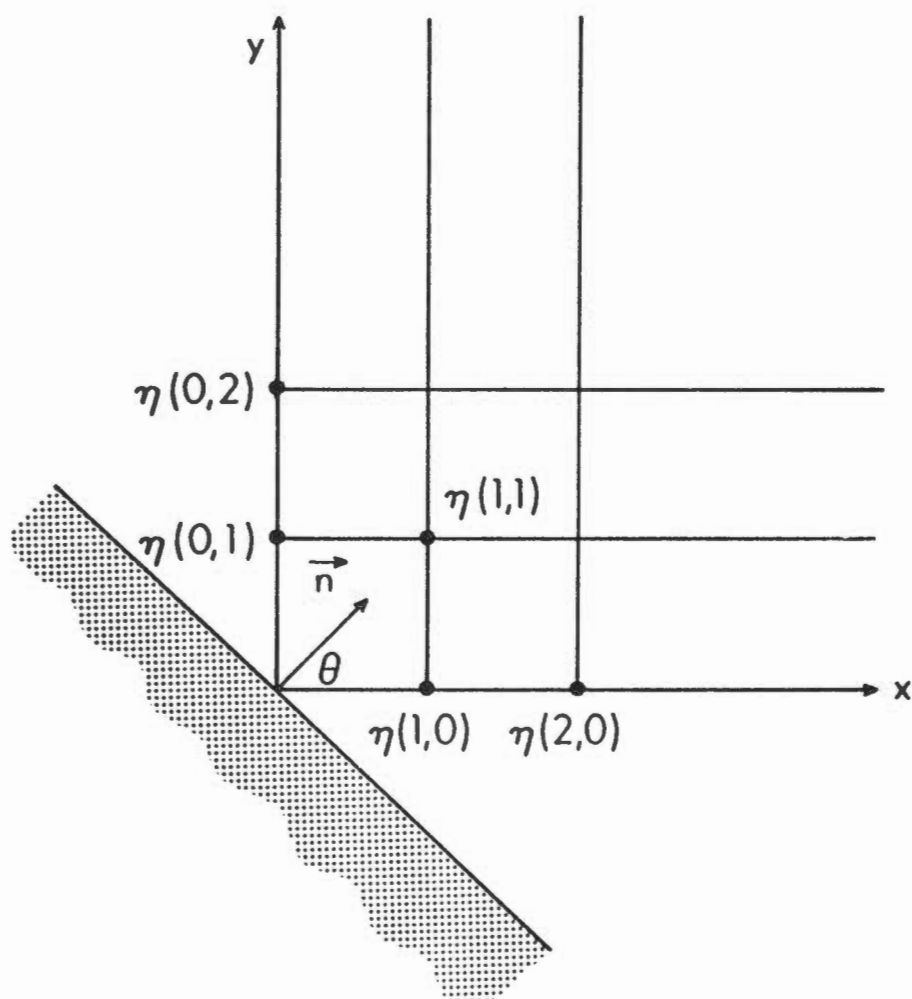


FIG. 2.2. Reflecting boundary condition.

By employing these formulas to the discretized grid and referring to Fig. 2.2, one gets

$$\eta_{1,0} = a_0 + a_1\Delta x + a_3\Delta x^2 \quad (x = \Delta x, y = 0)$$

$$\eta_{2,0} = a_0 + 2a_1\Delta x + 4a_3\Delta x^2 \quad (x = 2\Delta x, y = 0)$$

$$\eta_{0,1} = a_0 + a_2\Delta y + a_5\Delta y^2 \quad (x = 0, y = \Delta y)$$

$$\eta_{0,2} = a_0 + 2a_2\Delta y + 4a_5\Delta y^2 \quad (x = 0, y = 2\Delta y) \quad .$$

Noting that  $\eta_{0,0} = a_0$  and solving the above system of equations for  $a_0$ , yields

$$\eta_{0,0} = \frac{\Delta y(4\eta_{1,0} - \eta_{2,0}) \cos \theta + \Delta x(4\eta_{0,1} - \eta_{0,2}) \sin \theta}{3(\Delta y \cos \theta + \Delta x \sin \theta)} \quad . \quad (2.15)$$

Similar equations apply at each island boundary point for which the boundary orientation is characterized by the angle  $\theta$ .

To simulate a group of islands in the middle of an ocean, a transparent outer boundary must be created to allow reflected or scattered waves to radiate outward toward the open ocean. For consistency with the inner boundary, again only the water elevation is utilized in describing the open outer boundary. The basic assumption is that the wave profile does not change during one time step as it moves through the boundary, or in Lagrangian form

$$\frac{D\eta}{Dt} = 0 . \quad (2.16)$$

In traveling from  $t$  to  $(t + \Delta t)$  (Fig. 2.3), the particles move an  $x$  distance of  $u\Delta t$ . Each particle is marked with a value of  $\eta$ , which represents an intrinsic property associated with a particular fluid particle. That is, in the absence of friction, each surface disturbance will retain its value of  $\eta$ .

Equation (2.16) is just the inviscid advection equation which can be written (Shapiro and O'Brien, 1970) as

$$\frac{\partial \eta}{\partial t} + u \frac{\partial \eta}{\partial x} = 0 . \quad (2.17)$$

In the case of long waves, the intrinsic property is the wave elevation  $\eta$  which allows the wave to pass through the boundary at the Lagrangian wave speed  $\sqrt{gH}$  (analogous to  $u$ ). Thus the equation pertinent to the model becomes

$$\frac{\partial \eta}{\partial t} + \sqrt{gH} \frac{\partial \eta}{\partial x} = 0 . \quad (2.18)$$

The finite difference analogue of this condition can be expressed by the upstream differing method (Roache, 1972),

$$\frac{\eta_i^{n+1} - \eta_i^n}{\Delta t} = \sqrt{gH} \frac{\eta_{i-1}^n - \eta_i^n}{\Delta x} . \quad (2.19)$$

Equation (2.19) implies that the interior points are projected in time to obtain a boundary point. The interpolation parameter

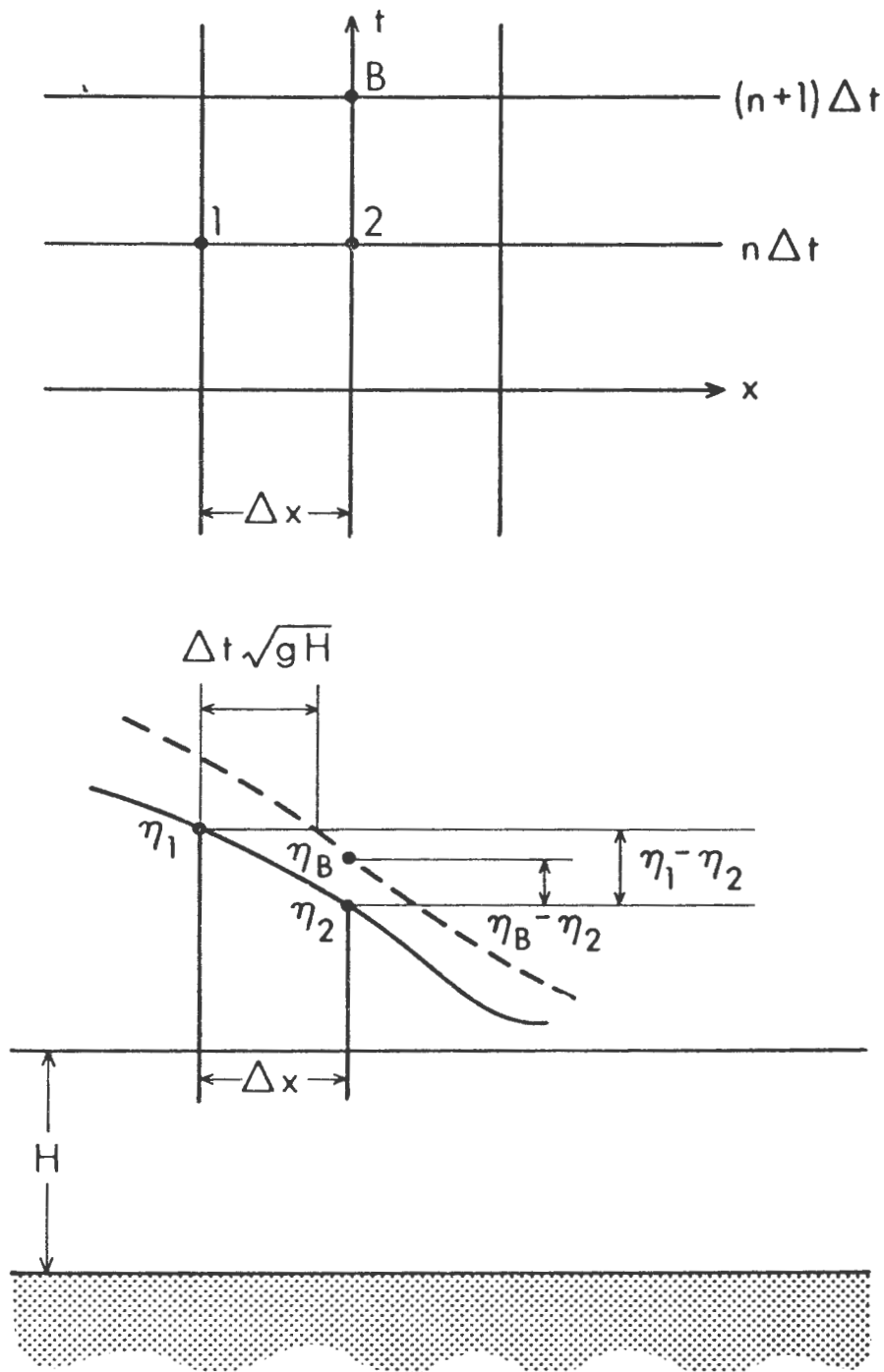


FIG. 2.3. The open boundary condition is graphically represented by the time scale (upper part) and the spatial scale (lower part). The water elevation  $\eta_B$  is calculated for time step  $(n+1)\Delta t$  by the upstream difference method and is represented by the dashed line in the lower part.

$$\frac{\Delta t \sqrt{gH}}{\Delta x} \quad (2.20)$$

is sometimes called the Courant number and makes the interpolation stable as long as

$$\frac{\Delta t \sqrt{gH}}{\Delta x} < 1 \quad (2.21)$$

(Roache, 1972). A graphical representation of the outflow boundary condition is shown in Fig. 2.3 and its finite difference analogue is

$$\eta_B^{n+1} = \eta_2^n + \sqrt{gH} \frac{\Delta t}{\Delta x} (\eta_1^n - \eta_2^n) . \quad (2.22)$$

For waves passing through a boundary which is normal to the  $y$  direction a similar analogue is computed using  $\Delta y$ . Using the constant depth region allows the waves to attain a condition in which they are essentially propagating outward without reflection by topographic features.

Having discussed the outflow boundary condition, one can now apply it with respect to a transparent boundary for scattered waves. The present model of linearized long waves allows scattered waves to be separated in the flow field by simple decomposition, or in terms of  $\eta$

$$\eta_{\text{scattered}} = \eta_{\text{total}} - \eta_{\text{incident}} .$$

The value of  $\eta_{\text{incident}}$  is determined by the input and represents the undisturbed passage of an incident wave through the model in the absence of topography. To provide an uncontaminated incident wave to



be used along the borders of the model, a one-dimensional canal is generated to be used as a reference for the incident wave (Fig. 2.4). The one-dimensional model is evaluated on the right-hand side of the grid assuming incident waves from the upper boundary. By setting the depth of the reference canal equal to the constant depth region of the model, the celerity of the waves in the canal is identically matched to the waves propagating along the borders of the model.

Having discussed all boundary conditions, one can see schematically how the model works (Fig. 2.4). The island is surrounded by transparent boundaries (to scattered waves), with the island being completely reflective. The region close to the transparent boundary is constrained to be of constant depth, as discussed earlier. The one-dimensional model on the right is the incident wave reference insuring the proper description of an undisturbed wave.

## 2.4 Confirmation of the Numerical Procedure

Verification of the numerical scheme described in the previous sections should be judged in terms of the agreement with those cases where analytic solutions of long waves interacting with islands exist. Boundary value scattering problems of simple geometry have been solved and are available in standard texts, as documented by Vastano and Reid (1966). In the cases to be considered, the diffraction pattern established at the shoreline is generated by the interaction of plane monochromatic waves given by:

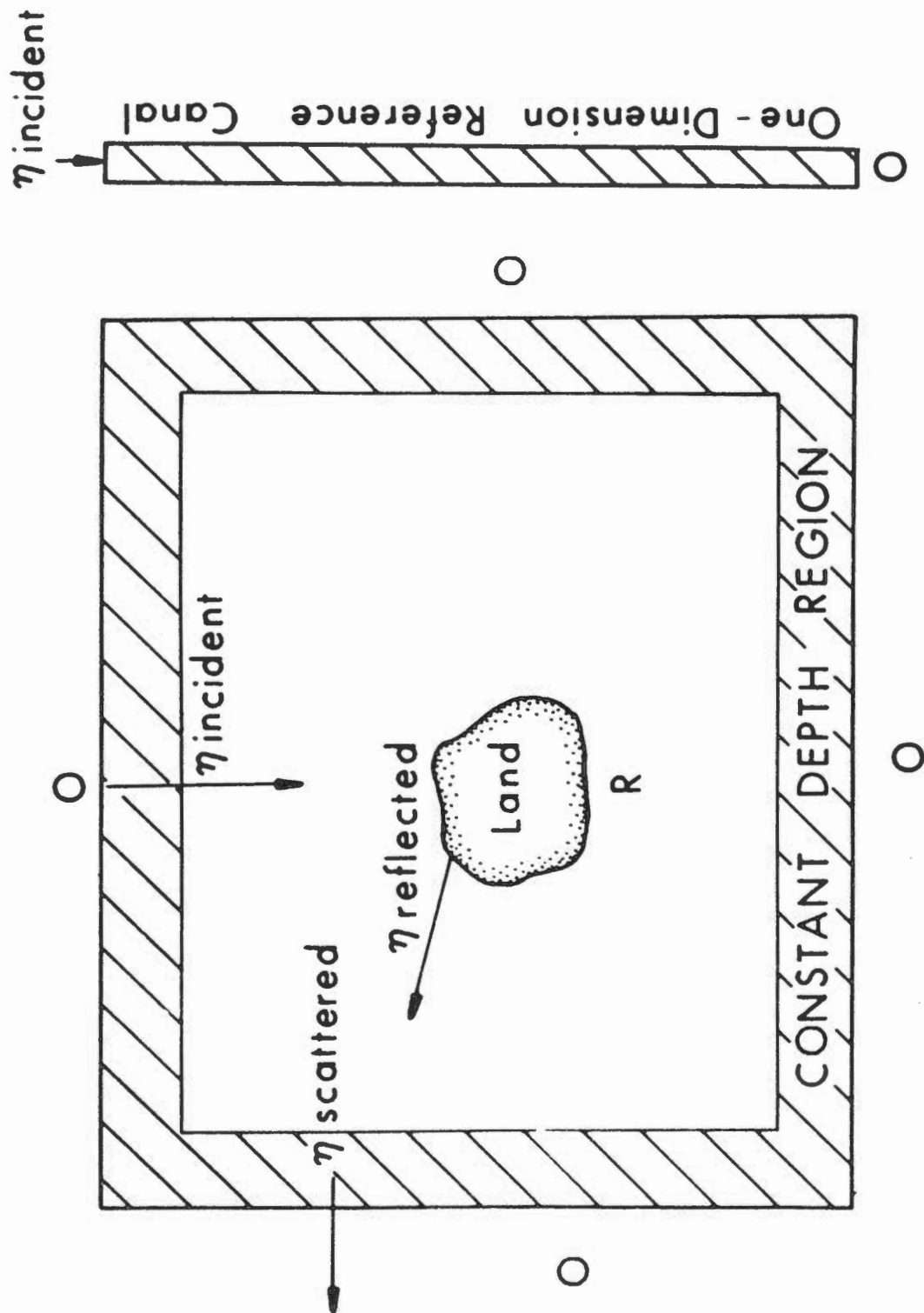


FIG. 2.4. Boundary configuration with one-dimensional reference canal.

$$\eta = e^{i(kr \cos \theta - \omega t)} \quad (2.23)$$

where  $k$  is the wave number,  $\omega$  is the angular frequency, the ratio  $\omega/k$  is the wave speed in the far field, and  $r$  is the radial distance from the center of a polar scheme.

Case 1. The simplest case is that of a cylindrical island of circular cross section (Fig. 2.5) in constant depth water. The water elevation at the shoreline is represented in polar coordinates with origin at the center of the island (Vastano and Reid, 1966) by:

$$\eta(r_0, \theta, t) = \left[ \sum_{n=0}^{\infty} \frac{2}{\pi k r_0} \frac{i^{n+1} \epsilon_n}{H'_n(kr_0)} \cos n\theta \right] e^{-i\omega t}, \quad (2.24)$$

where  $H_n$  refers to the  $n$ th order Hankel function ( $H_n = J_n + iY_n$ ),  $\epsilon_n$  assumes the value 1 for  $n = 0$  and the value 2 for  $n \neq 0$ , and the prime indicates a differentiation of the function with respect to its argument. By extracting real (a) and imaginary (b) parts of the bracketed part of (2.24) one obtains

$$\begin{aligned} a(\theta) &= \sum_{n=0}^{\infty} \operatorname{Re} \left[ \frac{2}{\pi k r_0} \frac{i^{n+1} \epsilon_n}{H'_n(kr_0)} \cos n\theta \right] \\ b(\theta) &= \sum_{n=0}^{\infty} \operatorname{Im} \left[ \frac{2}{\pi k r_0} \frac{i^{n+1} \epsilon_n}{H'_n(kr_0)} \cos n\theta \right]. \end{aligned} \quad (2.25)$$

The amplitude  $A(\phi)$  and phase  $\phi$  of the diffraction pattern at the island shoreline can be evaluated from the relations

$$A(\phi) = \sqrt{a^2 + b^2}$$

$$\phi(\theta) = \tan^{-1}(b/a) . \quad (2.26)$$

The numerical model was constructed to duplicate as nearly as possible the analytic model. Fig. 2.6 shows the Cartesian coordinate model of the cylinder (Fig. 2.5) and Table 2.1 gives the parameters and dimensions of the cylindrical island. The inner boundary condition allows each shoreline point to be oriented by a particular angle  $\theta$ . Thus, by appropriate matching of the angle orientation a circular island can be approximated. The model was designed so that the incident wave arrived from the  $180^\circ$  azimuth (top of Fig. 2.6) and, to save computational expense, symmetry was utilized. Therefore only one-half of the flow field was calculated. Plane monochromatic waves of 4 and 8 minutes were used as incident waves and the model was time-stepped until maximum amplitudes did not change in time. At this point, a periodic forced response was assumed to exist. The maximum amplitude of the waves from the numerical computations is plotted versus azimuth in Figs. 2.7 and 2.8, and is compared with the analytical solution to amplitudes on the shoreline. In these figures the azimuth exposed to the incident waves is  $180^\circ$ . Good agreement was found for both 4- and 8-minute periods; the deviation that occurred was attributed to the "octagonal" modeling of a cylinder.

Case 2. The case with variable depth is that of a parabolic island (paraboloid with a cap) (Fig. 2.9). The shoreline water elevation can be expressed by the following relationship, originally shown by Honma (1950) and adapted for computation by Vastano and Reid (1966):

TABLE 2.1. Parameters of verification comparison for the cylindrical island

| Analytic island       |       | Grid system  |
|-----------------------|-------|--|
| Radius ( $r_0$ )      | 19 km | Size of rectangle.... $46\Delta y \times 32\Delta x$ |
| Water depth ( $H_0$ ) | 4 km  | $\Delta x = \Delta y = 2.235$ km                     |
|                       |       | $\Delta t = 5$ seconds                               |

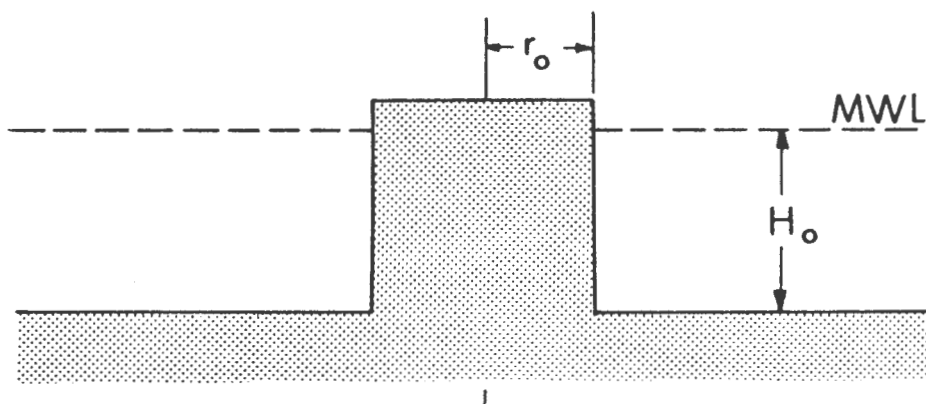


FIG. 2.5. Cylindrical island of radius  $r_0$  in constant depth ocean  $H_0$ .

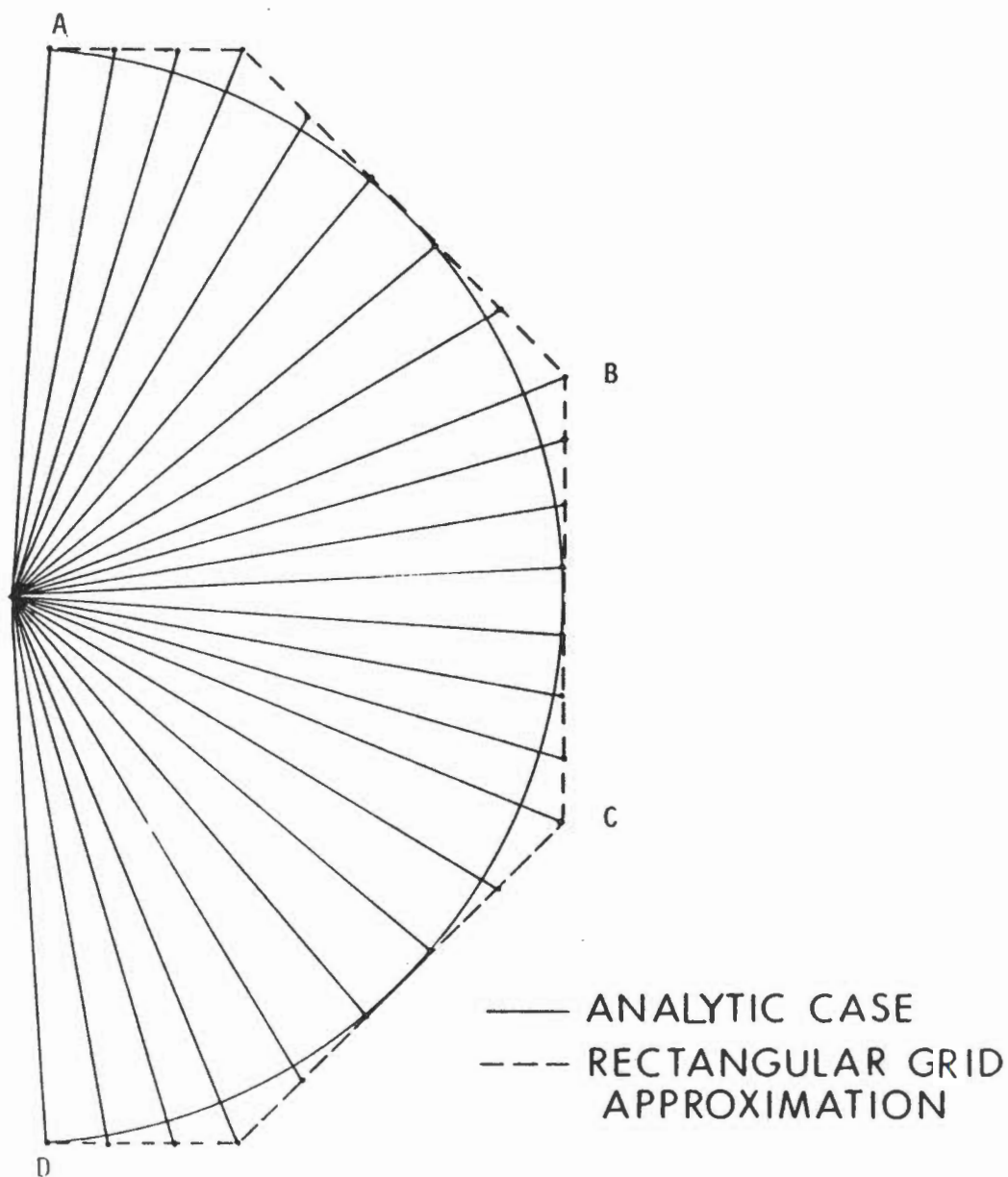


FIG. 2.6. Cartesian coordinate approximation of a cylindrical island where, for example, the value of  $\theta$  at A =  $86.5^\circ$ , B =  $22.5^\circ$ , C =  $-22.5^\circ$ , and D =  $-86.5^\circ$ .

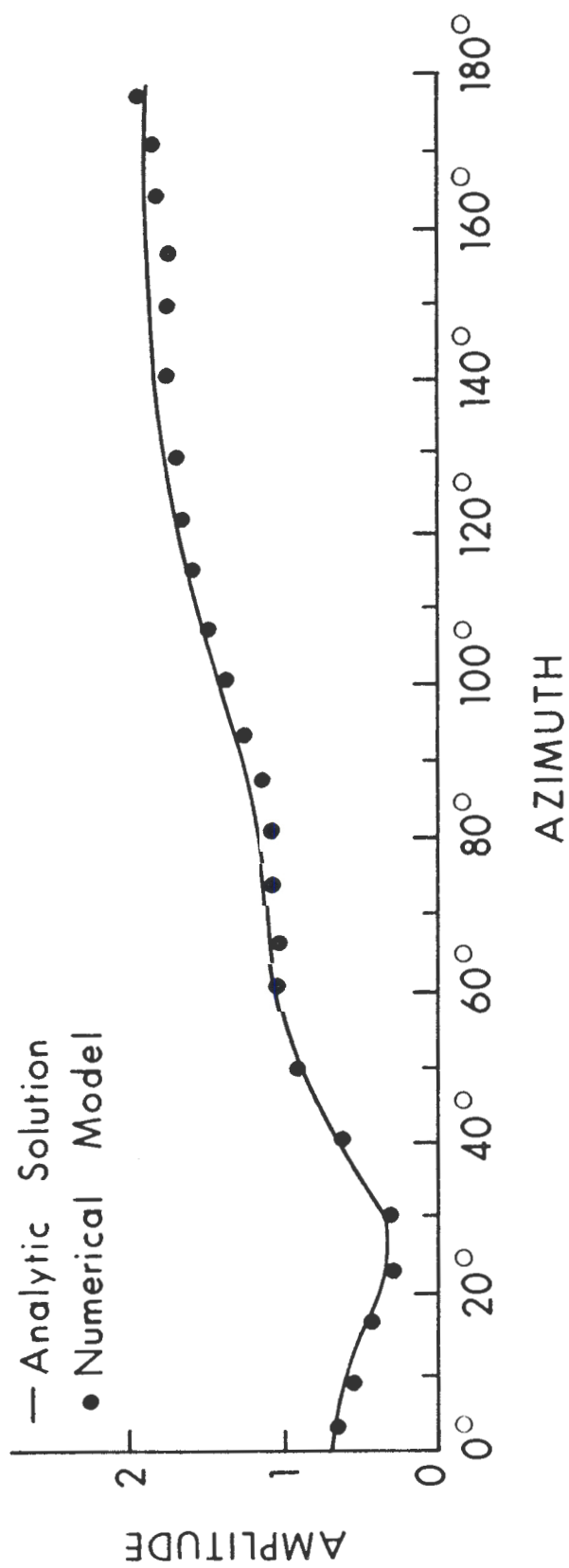


FIG. 2.7. Comparison of numerical model of cylindrical island with analytic solution for a 4-minute incident wave period. The incident side of the island is  $180^\circ$ .

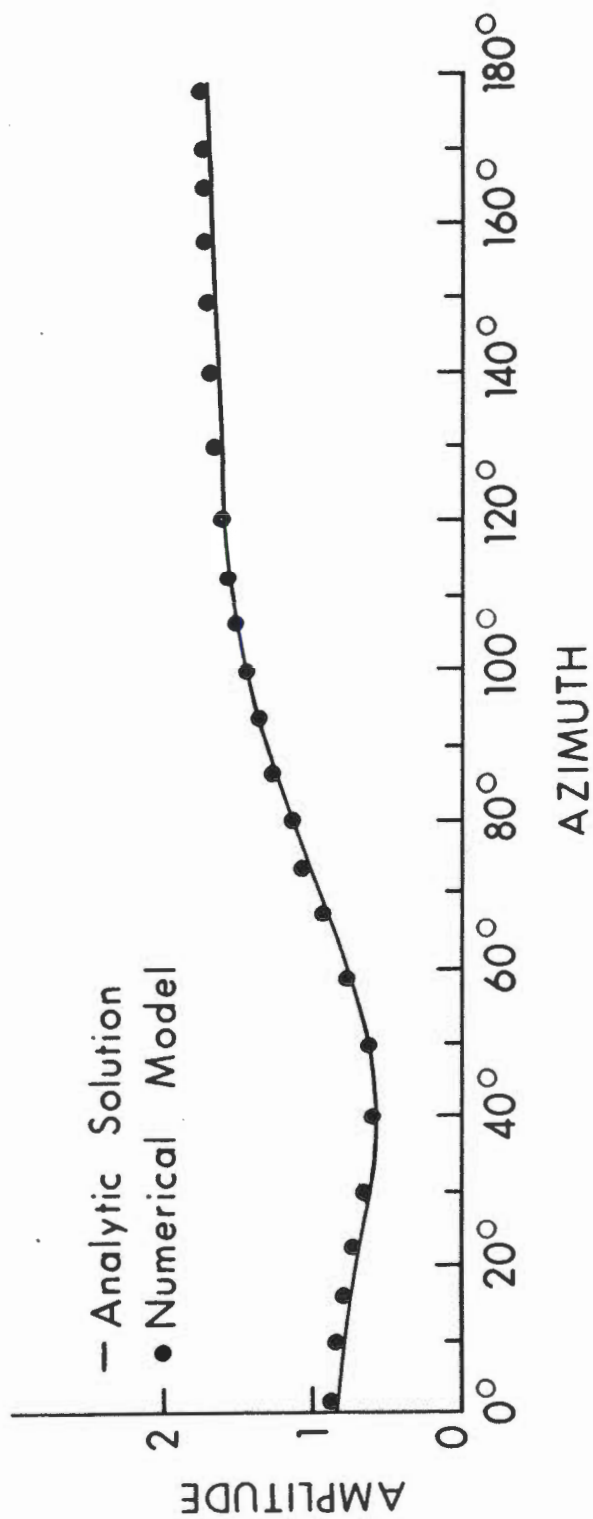


FIG. 2.8. As in Fig. 2.7 except for 8-minute incident wave period.



$$\eta(r_0, \theta, t) = \sum_{n=0}^{\infty} 2i^{n+1} \frac{\epsilon_n \rho^{\alpha_n}}{\pi A_n} \cos(n\theta) e^{-i\omega t}, \quad (2.27)$$

where

$$\rho = r_1/r_0,$$

$$\alpha_n = \sqrt{1 + n^2 - \tau^2},$$

$$A_n = -H_n(\tau)(\alpha_n^2 - 1) \sinh(\alpha_n s) + \tau H'_n(\tau)[\alpha_n \cosh(\alpha_n s) + \sinh(\alpha_n s)],$$

$$\tau = \frac{\omega r_1}{\sqrt{gH_1}},$$

and

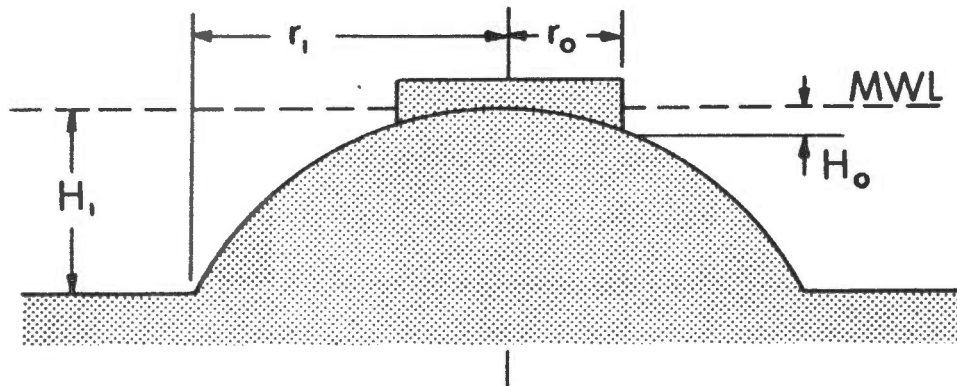
$$s = \ln \rho.$$

As in Case 1, the amplitude and phase of the diffraction pattern can be ascertained by using the real and imaginary parts of (2.27).

The numerical model was constructed with the parameters listed in Table 2.2. Again, the inner boundary condition approximated a circle, the incident plane monochromatic wave arrived from the 180° azimuth, and symmetry was utilized. The 8-minute period was used and the comparison is plotted in Figure 2.10. Good agreement is illustrated except for the bow side (incident side) of the cap, where the numerical model shows about a 4% deviation. The deviation is explained primarily by the depth field having been described by Cartesian coordinates. The failure of square grids describing circular bathymetry

TABLE 2.2. Parameters of verification comparison for the parabolic island

| Analytic island                        | Grid system   |
|--|---|
| Radius ( $r_0$ ).....10.5 km           | Size of rectangle.... $220\Delta y \times 96\Delta x$ |
| Shoreline depth ( $H_0$ ).... 0.446 km | $\Delta x = \Delta y = 1.176$ km                      |
|  | $\Delta t = 4$ seconds                                |
| <u>Radius of variable depth</u>        | <u>Coarse grid system</u>                             |
| Topography ( $r_1$ )..... 30 km        | Size of rectangle.... $116\Delta y \times 50\Delta x$ |
| Depth at $r_1$ ( $H_1$ )..... 4.014 km | $\Delta x = \Delta y = 2.222$                         |
|  | $\Delta t = 4$ seconds                                |

FIG. 2.9. Parabolic island of radius  $r_0$  with variable topography out to  $r_1$ .

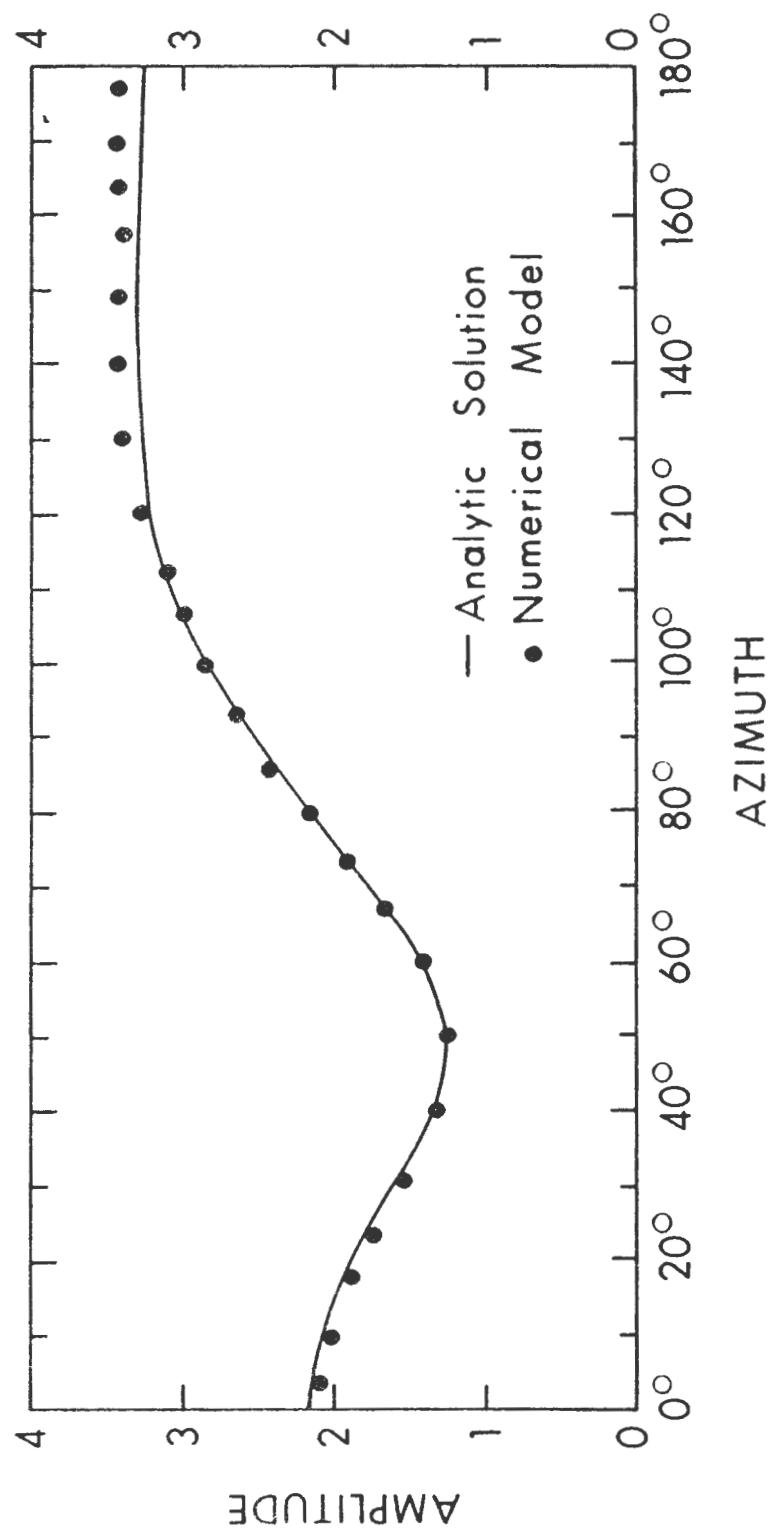


FIG. 2.10. Comparison of numerical model of parabolic island with analytic solution for an 8-minute incident wave period. The incident side of the island is 180°.

could result in the discrepancy. As a measure of sensitivity to the prescribed bathymetry, the paraboloidal island case was run using a flattened paraboloid ( $H = 0.4 r^2$  instead of  $H = 0.446 r^2$ ), and the resulting amplitudes varied about 10%. The analytic solutions also showed similar variations with the same bathymetric changes.

## CHAPTER III

## APPLICATION OF THE MODEL FOR RESPONSE ANALYSIS

3.1 Generalized Time Sequence Input

As noted previously, the goal of this investigation is to determine the response of the Hawaiian Islands to gravity waves over a band of frequencies in the tsunami range. A method for determining response patterns of single islands was presented by Longuet-Higgins (1967) and Knowles and Reid (1970). Longuet-Higgins (1967) examined the response of a circular island with a step sill analytically while Knowles and Reid (1970) determined the response with a numerical model. In both cases the trapped modes which induced resonances in the response pattern were excited by a sharp pulse.

Before we continue, an explanation of trapped modes is necessary. As long waves approach an island, the shallowing of the topography refracts the waves toward the island. The refraction captures waves of certain wave frequencies, i.e., the bathymetry creates a nearly continuous ray path around the island. Other waves may be trapped due to a reflection at the shoreline and a reflection at an abrupt bathymetric change. The reflection at the change in bathymetry is created by an angle of incidence exceeding the critical angle. Any combination of these trapped modes may exist for a single island with an arbitrary bathymetry.

Knowles and Reid (1970) demonstrated that a numerical excitation supplied by an incident wave sequence with a stipulated spectrum in the frequency domain could produce shoreline response spectra closely

approximating analytic solutions of island response. The input must be applied for a sufficient time span to insure that the shoreline response spectra become invariant with time. Thus, by appropriately describing the incident wave sequence, all resonances in the tsunami frequency range for a given island or island system can be excited.

The frequency-band-limited, generalized time sequence,  $H(k)$ , is defined by the Fourier Series

$$H(k) = \sum_{j=0}^M A(j) \cos (2\pi j(k-KS)/NT) \quad (3.1)$$

where  $NT$  is the maximum number of time intervals,  $M$  is the maximum number of frequency intervals,  $k = t/\Delta t$ ,  $j = f/\Delta f$  are integers, and  $KS$  is a constant determining the number of time steps the pulse peak is delayed from  $t = 0$ . The coefficients  $A(j)$  are calculated using the relation

$$A(j) = e^{-\beta j^2} \quad (3.2)$$

where  $\beta = 9/2M^2$ , i.e., with a standard deviation of  $M/3$ . The shape of the input resembles a wide, high-amplitude pulse. For example, the incident pulse used for the Hawaiian model was 305.6 km wide with 30.0-m peak amplitude.

### 3.2 Verification of the Response Technique

Verification of the numerical response study was achieved by agreement with the analytic solution of the response of the parabolic island as shown in Fig. 2.7 (page 25). Muirhead (1967) determined

analytically the response of the parabolic island by examining the average potential energy of the water elevation at the shoreline. The energy is proportional to  $\overline{|\eta(r_0, \theta, t)|^2}$  where the average is with respect to  $\theta$  over the range 0 to  $2\pi$ . By using (2.27) and the orthogonality property of trigonometric functions, it can be shown that

$$E = \overline{|\eta(r_0, \theta, t)|^2} = \sum_{n=0}^{\infty} \frac{4\rho^2 |\alpha_n|^2 \epsilon_n}{\pi^2 |A_n|^2} \quad (3.3)$$

where  $E$  signifies the mean energy of the waves at the shoreline relative to incident waves. The variables  $\alpha_n$  and  $A_n$  are a function of  $\omega$  (angular frequency).

A plot of analytically determined  $E$  versus frequency for the parabolic island described in Table 2.2 (page 28) is represented by the upper solid line in Fig. 3.1. The peaks in energy show resonance of selected frequencies trapped by the bathymetry of the island. The general shape of the response pattern is an increase in energy with frequency and a narrowing of the resonance peaks with frequency. Physically, the number of waves trapped by the bathymetry increases as the wavelength decreases (frequency increases), allowing more energy to be captured. Wavelength reduction accentuates the energy amplification of selected frequencies and results in a narrowing of resonance peaks.

To simulate the analytic response, the following numerical procedure was implemented: (1) time step the generalized time sequence input until the output spectrum becomes invariant (equilibrium),

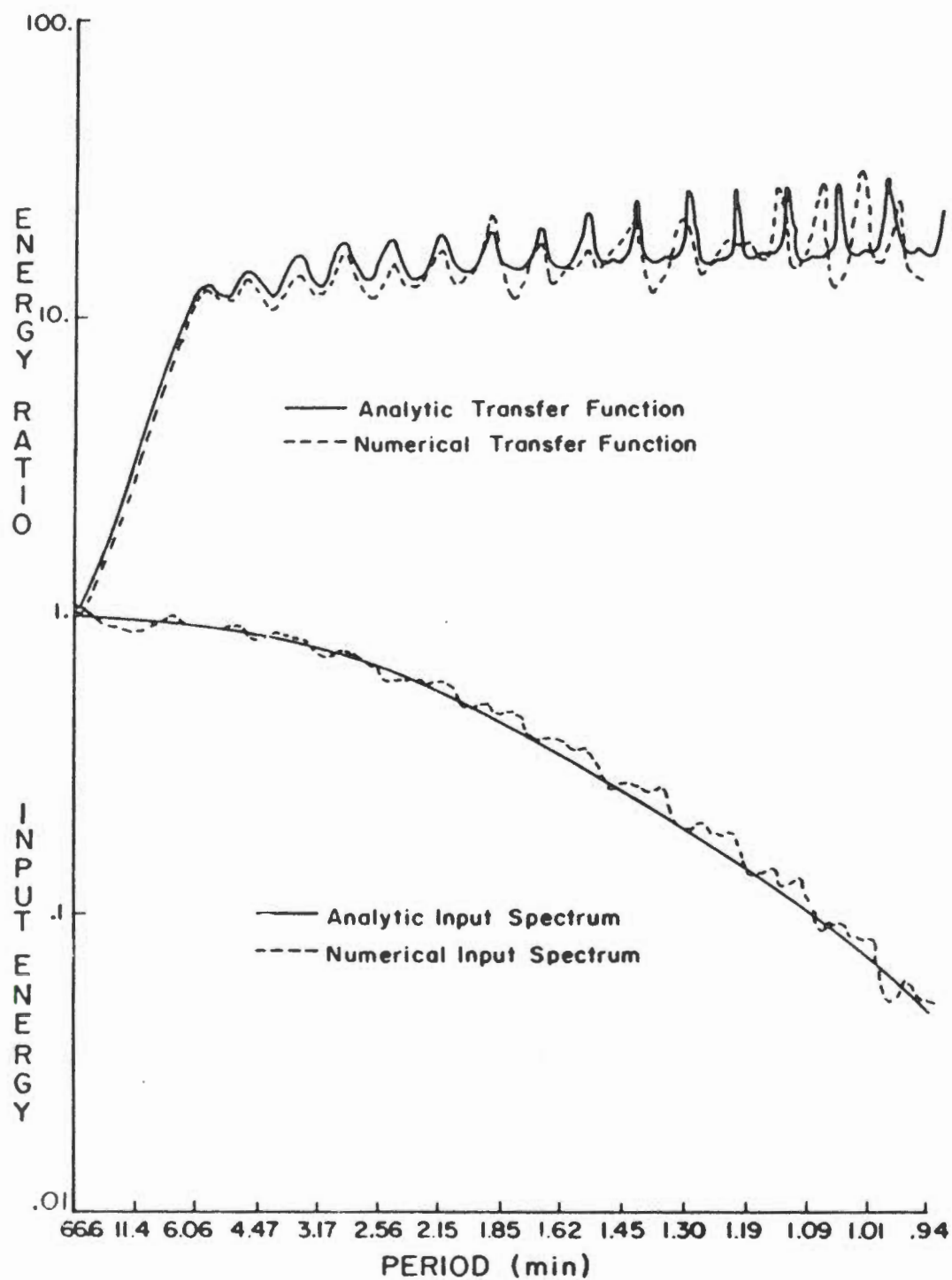


FIG. 3.1. Comparison of numerical and analytic transfer functions (upper part) for the parabolic island of Fig. 2.9 and comparison of numerical and analytic input spectra (lower part).



(2) record and Fourier analyze the time history of the water elevation for each shoreline grid point, (3) establish a transfer function by ratio of the spectrum of output to that of input, and (4) average the transfer function around the island. The numerical transfer function was obtained by the ratio of numerical output spectrum to that of numerical input spectrum. To secure the proper numerical input spectrum, a hydrograph, recorded in the center of a constant depth model (4014 m) with identical parameters, dimensions, and input as the parabolic test case, was Fourier analyzed. The parameters of  $H(k)$  in (3.1) and (3.2) were  $NT = 1000$ ,  $M = 100$ ,  $KS = 46$ , and  $\Delta t = 4.0$  sec.

The upper dashed line in Fig. 3.1 (page 34) represents the numerical transfer function while the lower dashed line illustrates the numerical input spectrum. The lower solid line shows the analytic input spectrum. Examination of the comparison between the numerical and analytic transfer functions reveals fairly good agreement for periods of 1.09 minutes and greater. At periods below 1.09, a shift develops in the numerical response that may be explained by the rectangular grid approximation of circular bathymetric contours. The period (or frequency) at which the numerical response separates from the analytic response is also related to the grid size of the model. If it is assumed that four grid points are necessary to describe a wave, then dividing  $4\Delta x$  by the slowest wave speed (shallowest depth) should yield the lowest period describable by a given grid size. For the numerical parabolic test, the grid spacing is 1176 m and the slowest wave speed is 69.0 m/sec, indicating the

lowest predictable period as 1.15 minutes. The parabolic test case is close to the  $4\Delta x$  criterion.

To investigate the changes in response accuracy with grid size, a parabolic case with less resolution was considered. The parameters of the coarse parabolic model are found in Table 2.2 (page 28). Except for a change in grid spacing from 1176 to 2222 m, the procedure followed in the coarse model duplicated the first run. The upper and lower dashed lines of Fig. 3.2 show the analytic spectra.

Separation of the numerical response of the coarse model from the analytic takes place at a period of 1.75 minutes. By using the  $4\Delta x$  criterion, the lowest period describable at the shoreline is 2.23 minutes. If a  $3\Delta x$  rule were applied, the lowest period would be 1.67 minutes. The coarse model yields a better cut-off frequency than the first model since the departure from the analytic curve occurs at a lower period relative to grid size. Improvement in the cut-off frequency could be explained by the bathymetric difference between the two models. Even though the bathymetry has the same parabolic shape in both models, the coarse grid has fewer shallow water grid points that affect reduction in the residence time of waves trapped in shallow water. Instead, the waves remain longer in deeper water with higher phase speed, which in turn reduces the value of the lowest period for a given grid size.

The dual response study enables the cut-off frequency of the numerical scheme to be determined. The coarse and regular grid response analyses indicate that the generalized time sequence is appropriate for exciting the modes trapped by island bathymetry, and

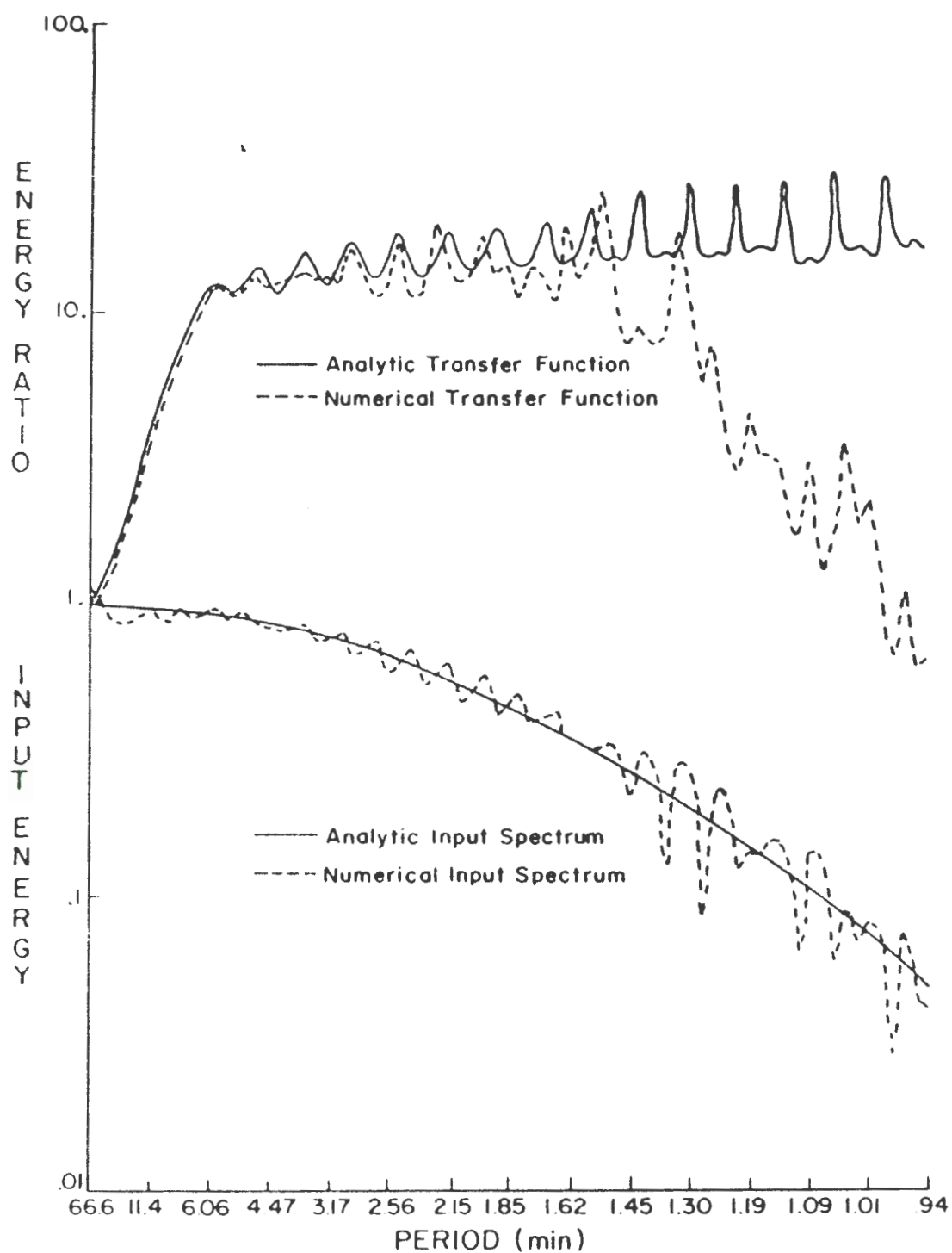


FIG. 3.2. Comparison of coarse numerical and analytic transfer functions (upper part) for the parabolic island of Fig. 2.9 and comparison of numerical and analytic input spectra (lower part).

that the cut-off of the frequency response lies between the  $3\Delta x$  and  $4\Delta x$  criteria for the shallowest depth in the system.

## CHAPTER IV

A STUDY OF THE RESPONSE OF THE HAWAIIAN ISLANDS TO A  
TSUNAMI APPROACHING FROM ALASKA4.1 The Hawaiian Islands Numerical Model

Since the speed of long waves is proportional to the square root of the depth of water, careful attention was given to the accuracy of the depth description in the Hawaiian Islands model. National Ocean Survey chart 4102, the most precise sounding information of the Hawaiian Islands available to the general public, was used to create the modeled underwater bathymetry of the islands. To convert the soundings for use in a digital computer, a grid was formed by a spline interpolation technique (Bernard, 1973) allowing a field of arbitrary (in the x-y plane) spaced points to be interpolated onto a specified grid. The numerical spline interpolation was programmed by Taylor, Richards, and Halstead (1971) and utilizes a second order, piecewise, polynomial fit.

To create the Hawaiian Islands model, the 4613 arbitrary (in the x-y plane) soundings on NOS chart 4102 were digitized and splined onto a 5.5-km square grid. Because a constant depth region was required for proper rendition of the open boundary condition, a flat skirt was merged into the outer edge of the topographic portion representing chart 4102. Fig. 4.1 illustrates a plan view of the model including the topographic region surrounded by a constant depth region. The model encloses an area of approximately 6° latitude by 10° longitude and is composed of 26,000 square grids. A

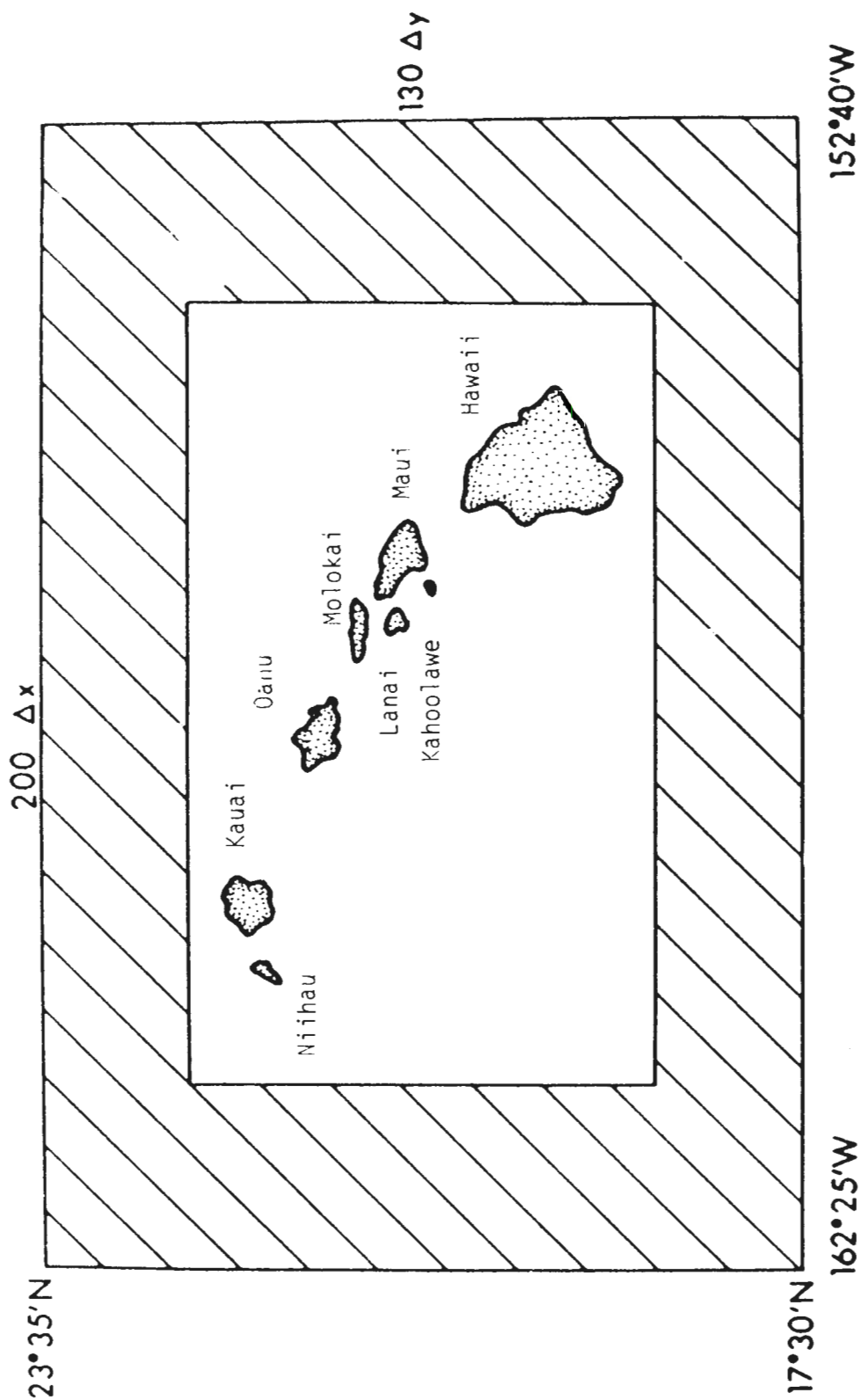


FIG. 4.1. Hawaiian Islands model showing topographic area with surrounding constant depth region.

perspective view of the topography of the model region is shown in Fig. 4.2. Since cathode ray tube graphics are limited, each square in Fig. 4.2 represents nine grid points of the actual model. Each outer boundary grid point allows scattered waves normal to the boundary to pass unobstructed, and each inner boundary grid point totally reflects all waves.

#### 4.2 Results of the Hawaiian Islands Response to Generalized Input Approaching from Alaska

Following the procedure described in Section 3.2, a generalized time sequence input  $H(k)$  in (3.1), approaching from  $180^\circ$  azimuth (normal to the upper boundary of Fig. 4.1) with parameters ( $NT = 2048$ ,  $M = 70$ ,  $KS = 46$ , and  $\Delta t = 15$  sec) was time-stepped into the Hawaiian Islands model. A transfer function for each island shoreline point was obtained by dividing the output spectrum by a numerical input spectrum derived from a constant depth model (4550 m) of the same dimensions. The analytic and numerical input spectra are compared in Fig. 4.3. The frequency cut-off of the response analysis is bracketed by the limits of the numerical scheme, i.e., upper period limit  $\frac{4\Delta x}{\sqrt{gH_{\text{minimum}}}}$  and lower period limit  $\frac{3\Delta x}{\sqrt{gH_{\text{minimum}}}}$  as discussed in Section 3.2. For the case of the Hawaiian Islands model with 50 m as the shallowest depth, the period cut-off lies between 16.74 minutes and 12.55 minutes, respectively.

To evaluate the response of the island system, an overall system response was calculated by averaging the 235 shoreline grid point

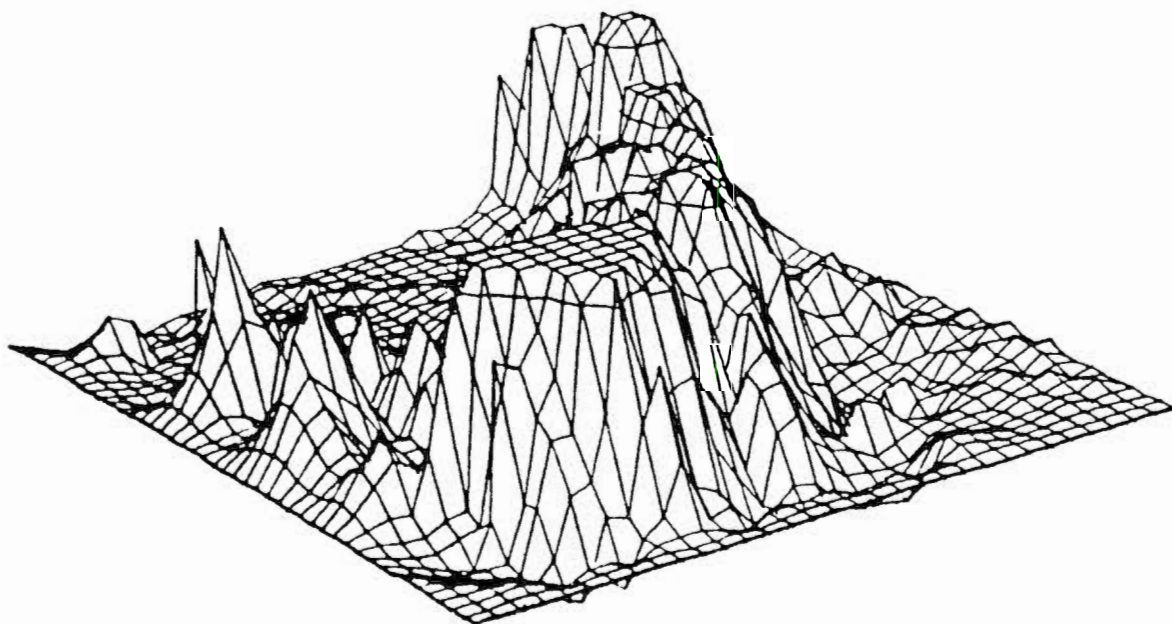


FIG. 4.2. Perspective view of the Hawaiian model topography looking from the southeast. Each grid point represents nine grid points of the actual model.



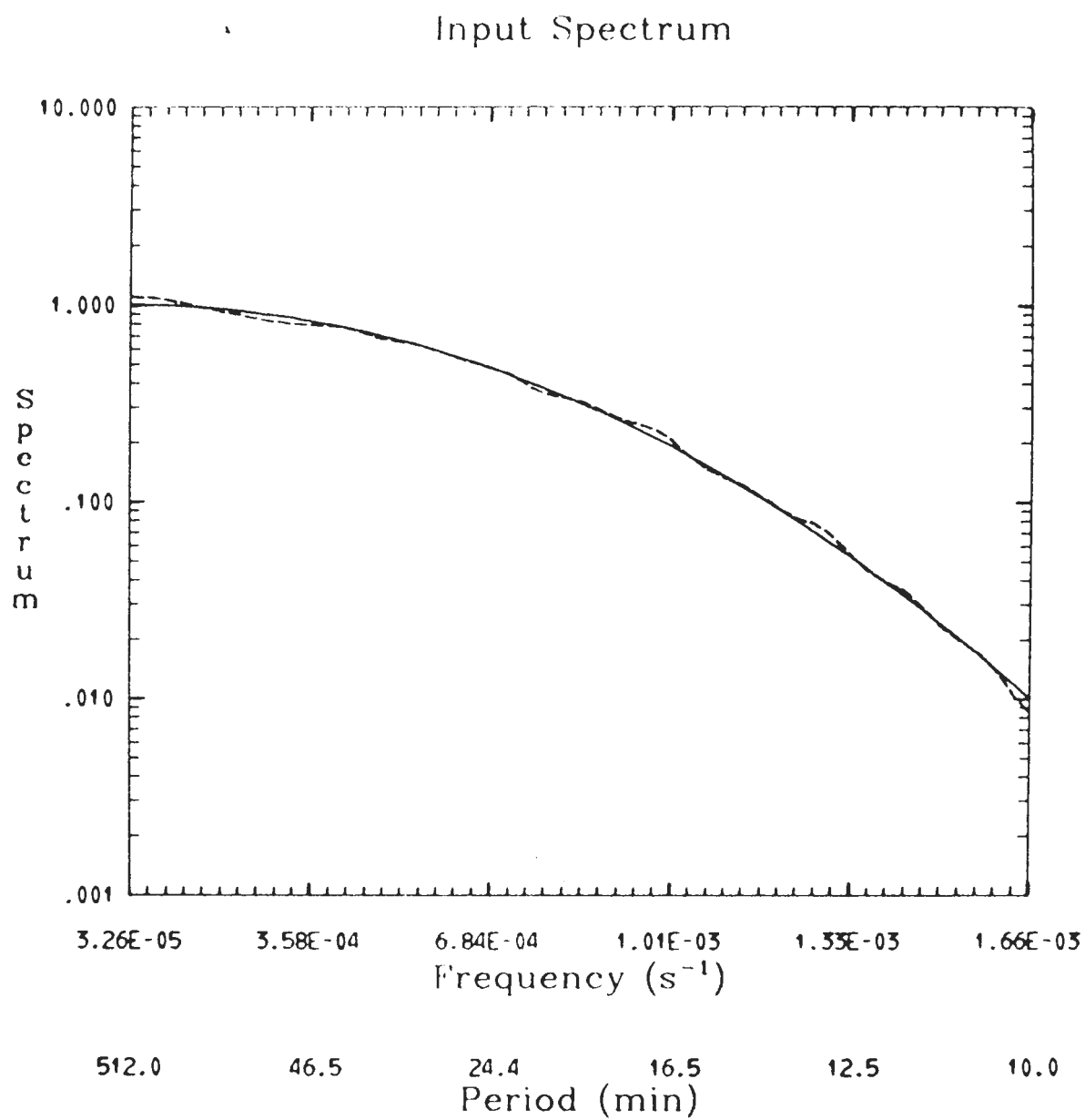


FIG. 4.3. Comparison of numerical and analytic input spectra for the Hawaiian model. The solid line is the analytic curve and the dashed line is the numerical model equivalent.

transfer functions over each frequency band. As shown in Fig. 4.4, the system average transfer function indicates nine resonant peaks between 512.0- and 12.5-minute periods. The most energetic period is 14.2 minutes followed by 17.7, 16.0, 12.5, 36.6, 20.5, 25.6, 56.9, and 73.1 minutes, respectively. The longest period had the least energy associated with it, indicating little excitation in periods longer than 512 minutes. Comparison of Fig. 4.4 with the parabolic island response (Fig. 3.1, page 34) reveals a similar overall pattern, i.e., the response is unity at the longest period and rises to a plateau with resonance peaks fluctuating from this level.

In addition to the system average, individual island averages were determined. The individual island averages, shown in Figs. 4.5 through 4.12, were helpful in analyzing each island separately and in evaluating each island's contribution to the system average. Table 4.1 lists the values of the response of individual islands as well as the value of the system average response for resonant periods that appear in Fig. 4.4. The table also indicates resonant peaks (and their value) for periods other than the system average and identifies those islands having these additional peaks. Examination of Table 4.1 is very useful in ascertaining and interpreting resonant peaks associated with specific islands. For example, the 17.7-minute period resonance in Fig. 4.4 is associated with Kauai only, the 36.6-minute period peak is a contribution of the Molokai, Lanai, Maui, Kahoolawe island group, and the 16.0-minute resonance is an almost equal contribution of all islands except Kauai.

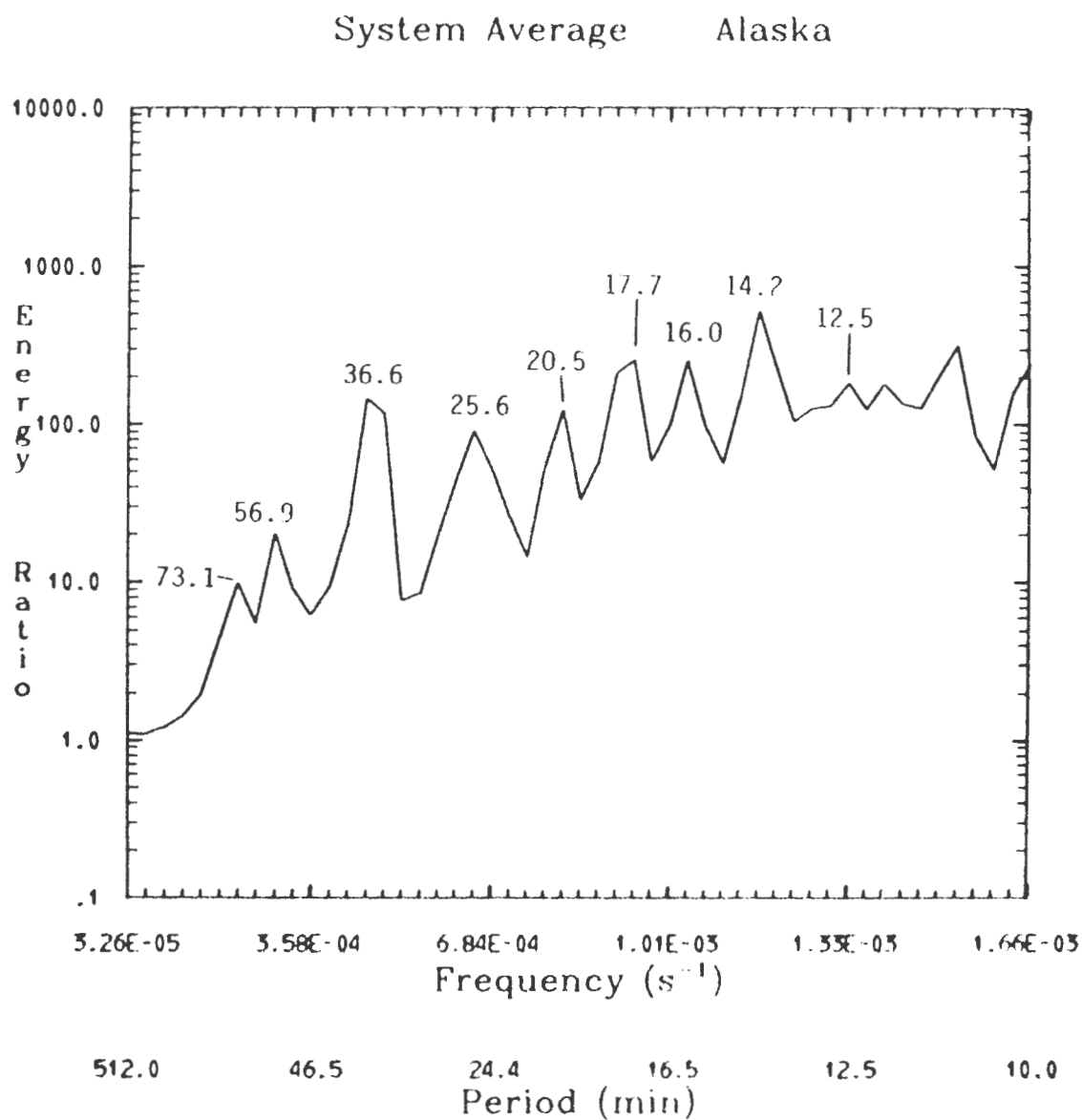


FIG. 4.4. Average of all shoreline transfer functions of the Hawaiian model for a tsunami originating in the Alaska region. Numbers above the peaks represent the associated period in minutes.

# Niihau Average - Alaska

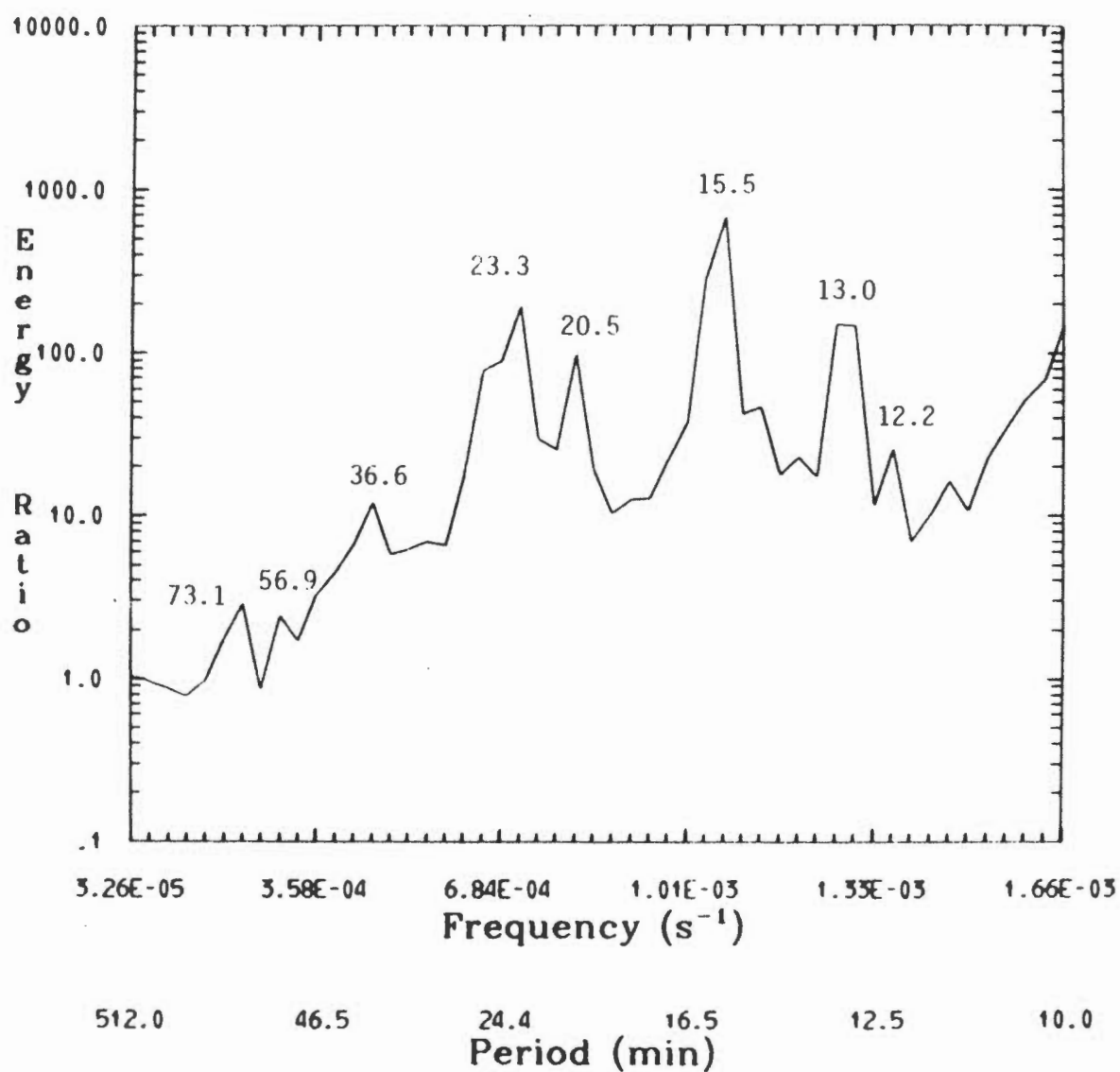


FIG. 4.5. Average of transfer functions around Niihau. Numbers above the peaks represent the associated period in minutes.

# Kauai Average - Alaska

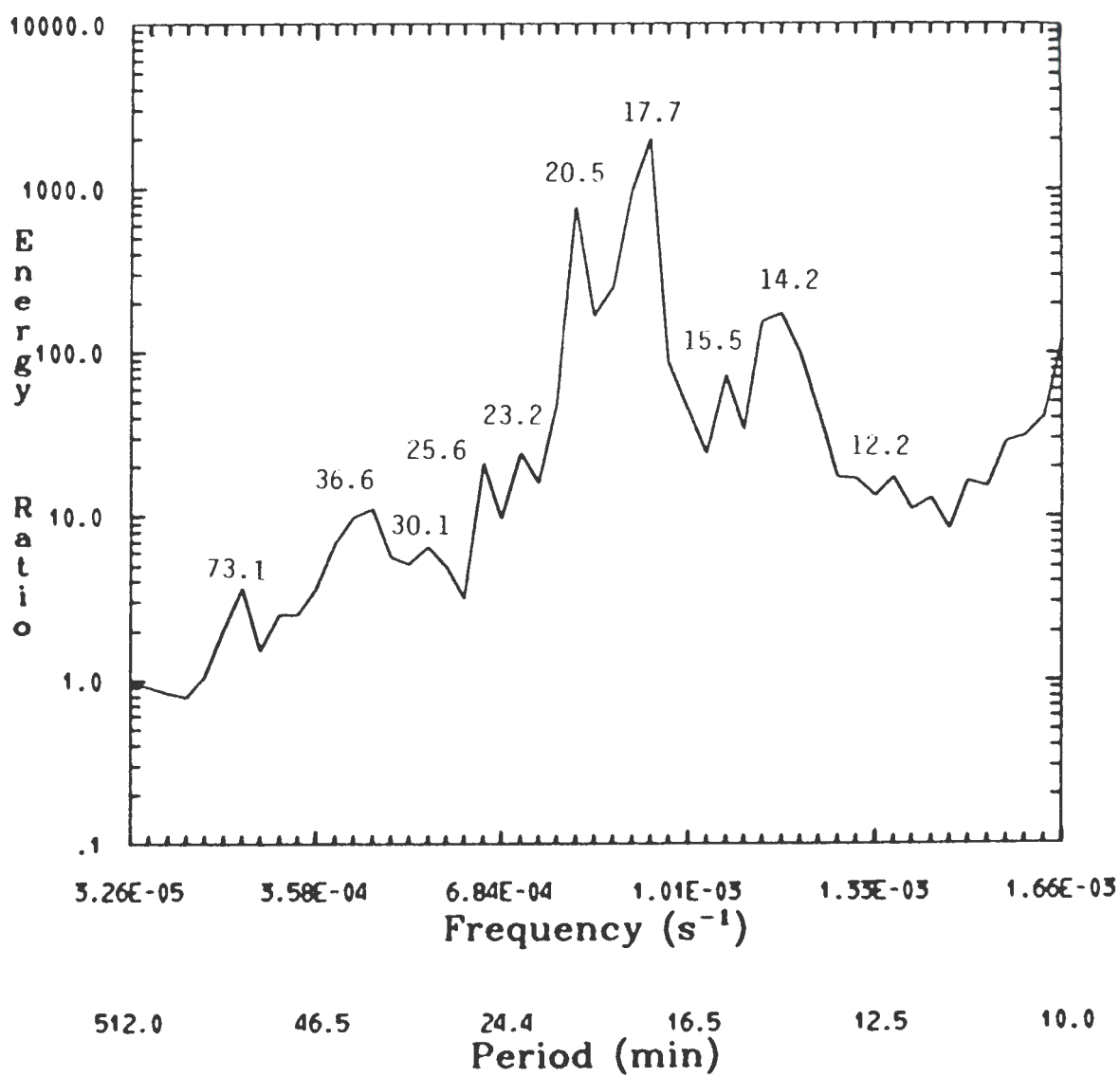


FIG. 4.6. As in Fig. 4.5 except around Kauai.

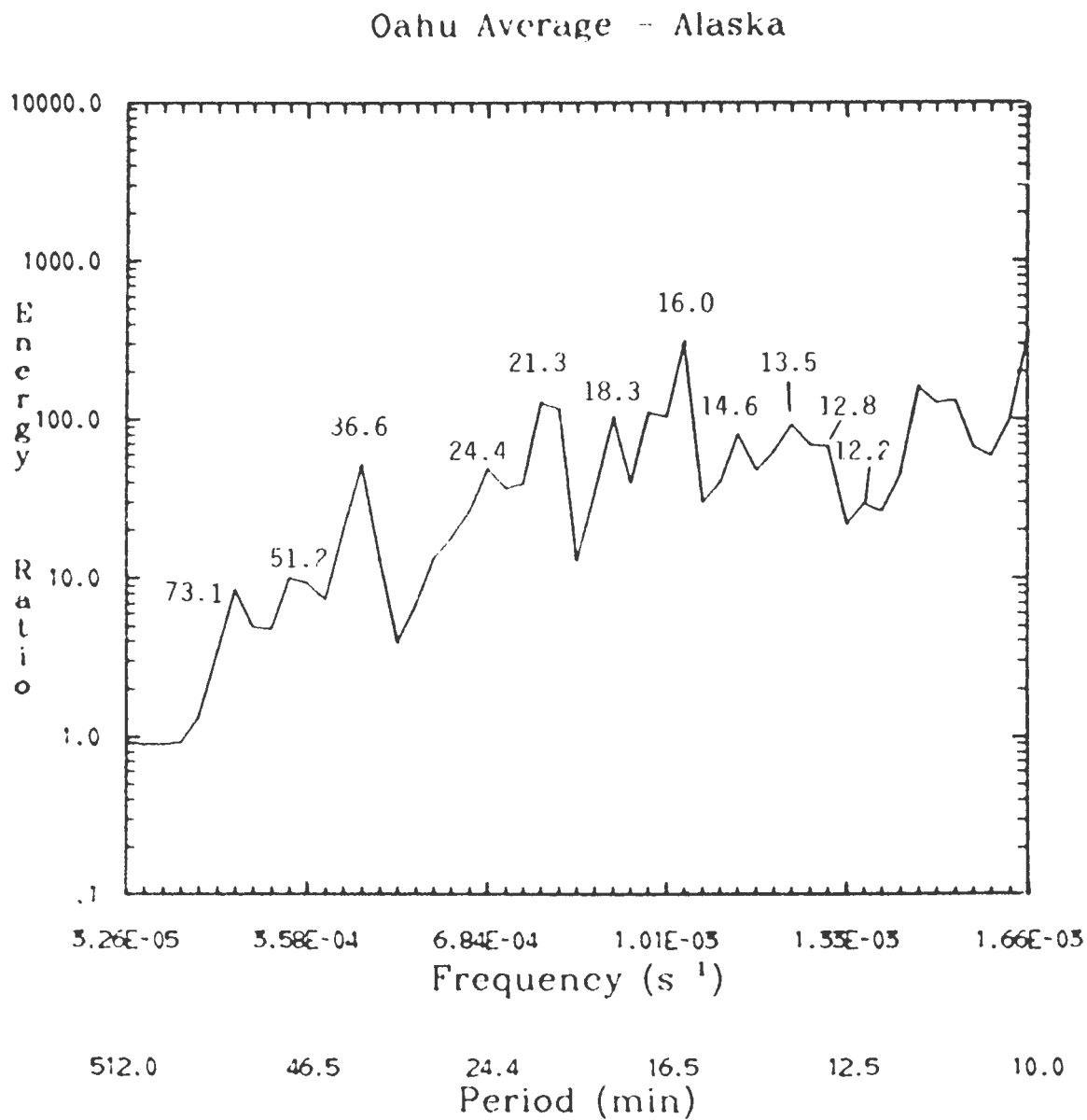


FIG. 4.7. As in Fig. 4.5 except around Oahu.

# Molokai Average - Alaska

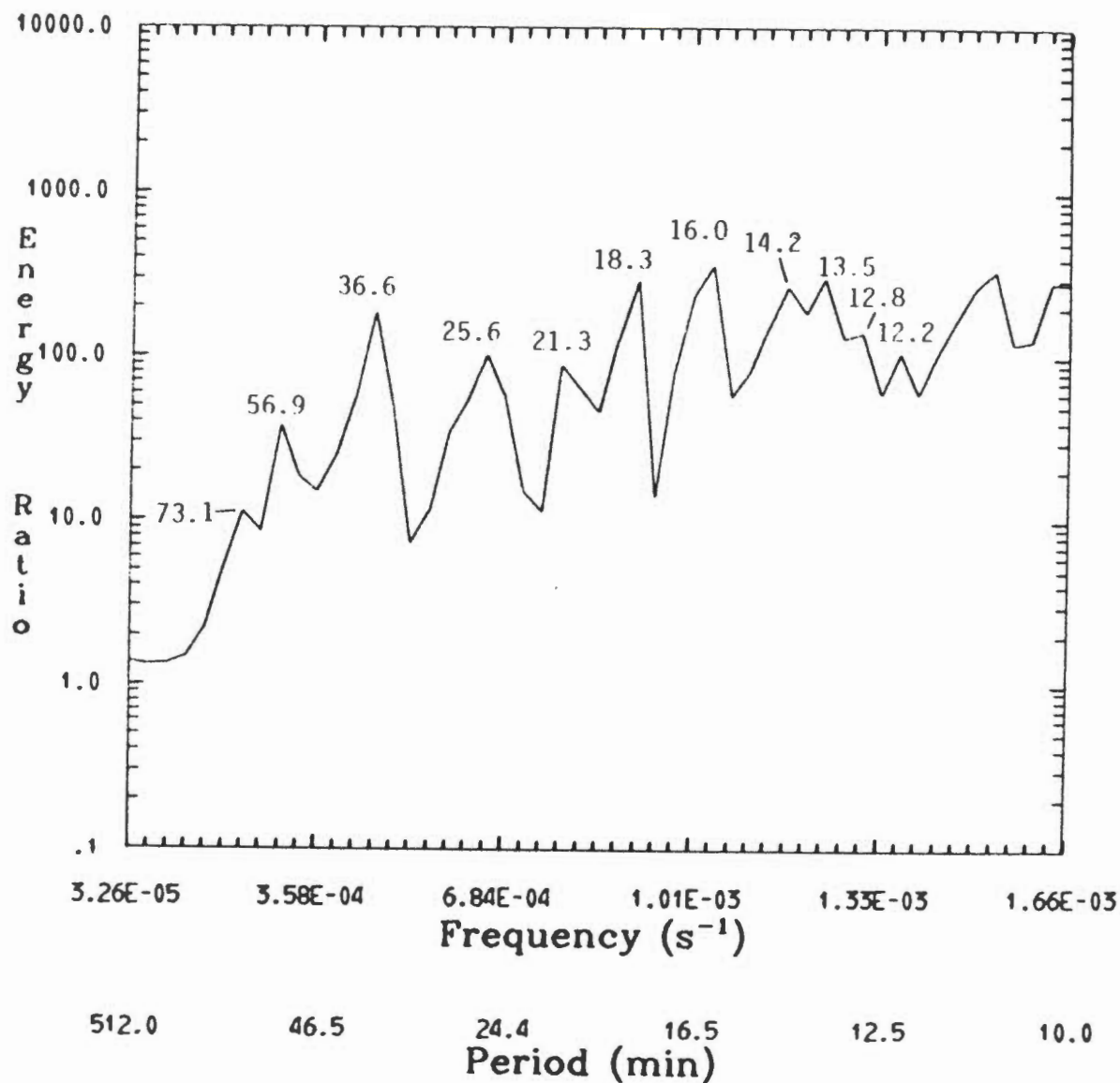


FIG. 4.8. As in Fig. 4.5 except around Molokai.

## Lanai Average - Alaska

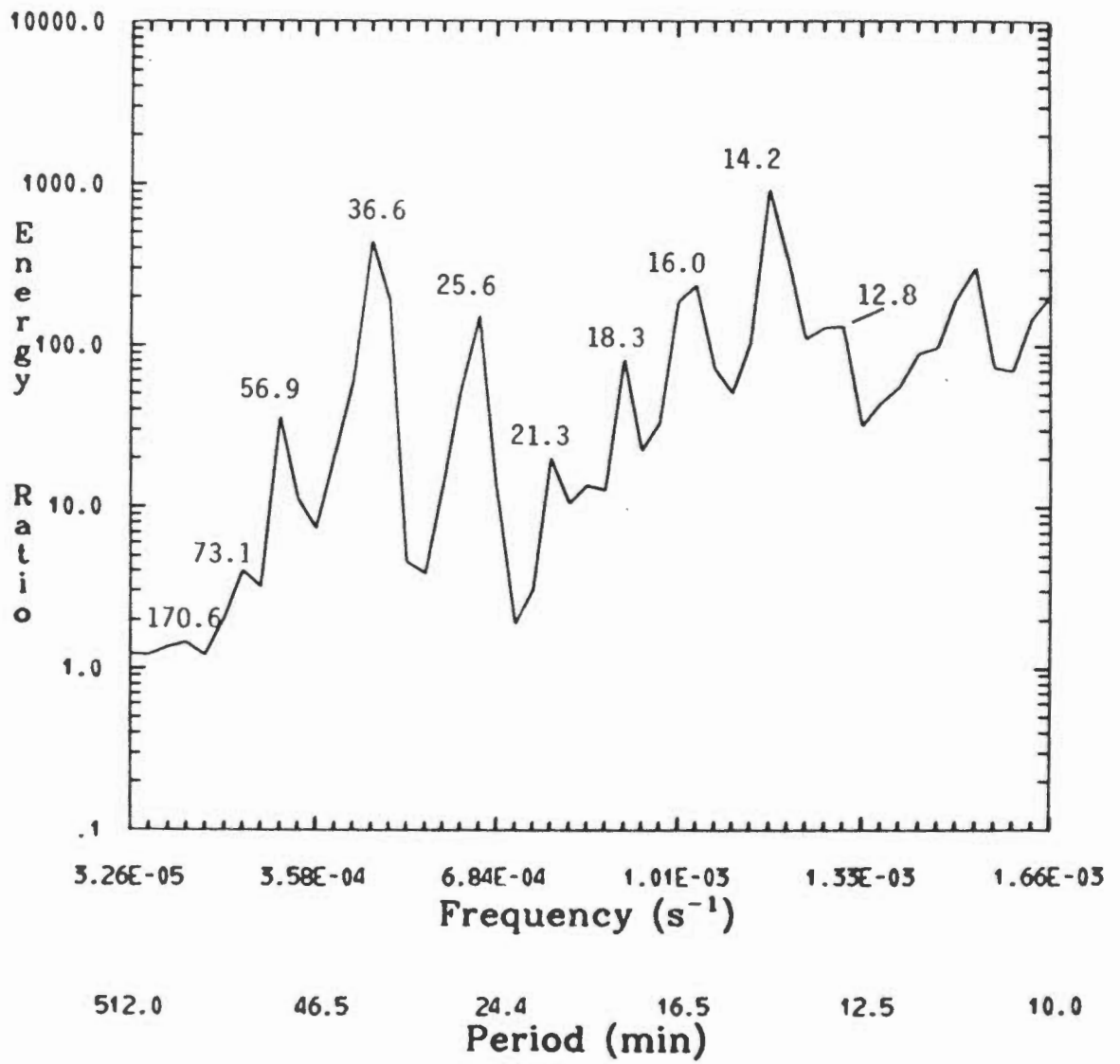


FIG. 4.9. As in Fig. 4.5 except around Lanai.



# Kahoolawe Average - Alaska

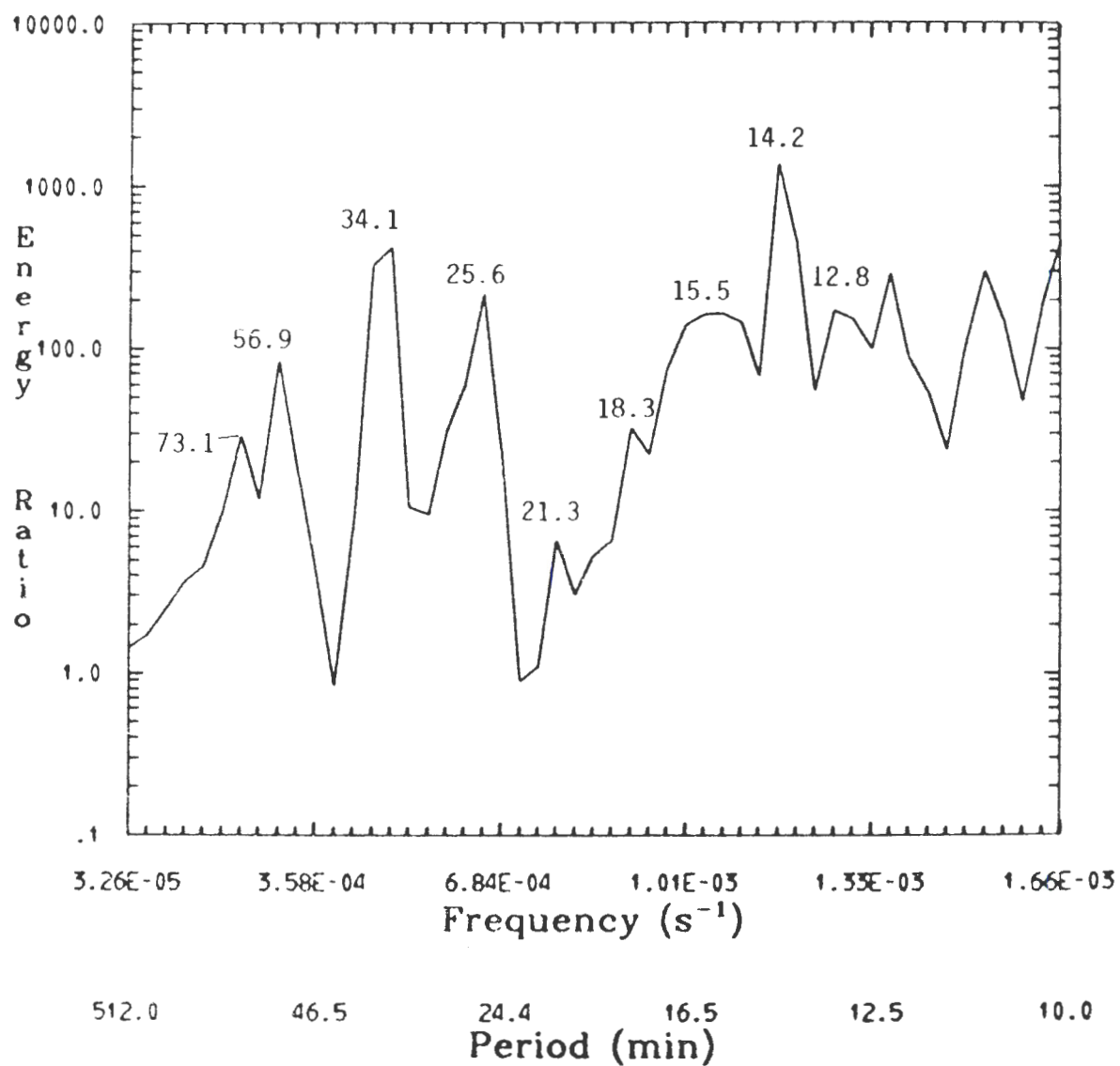


FIG. 4.10. As in Fig. 4.5 except around Kahoolawe.

## Maui Average - Alaska

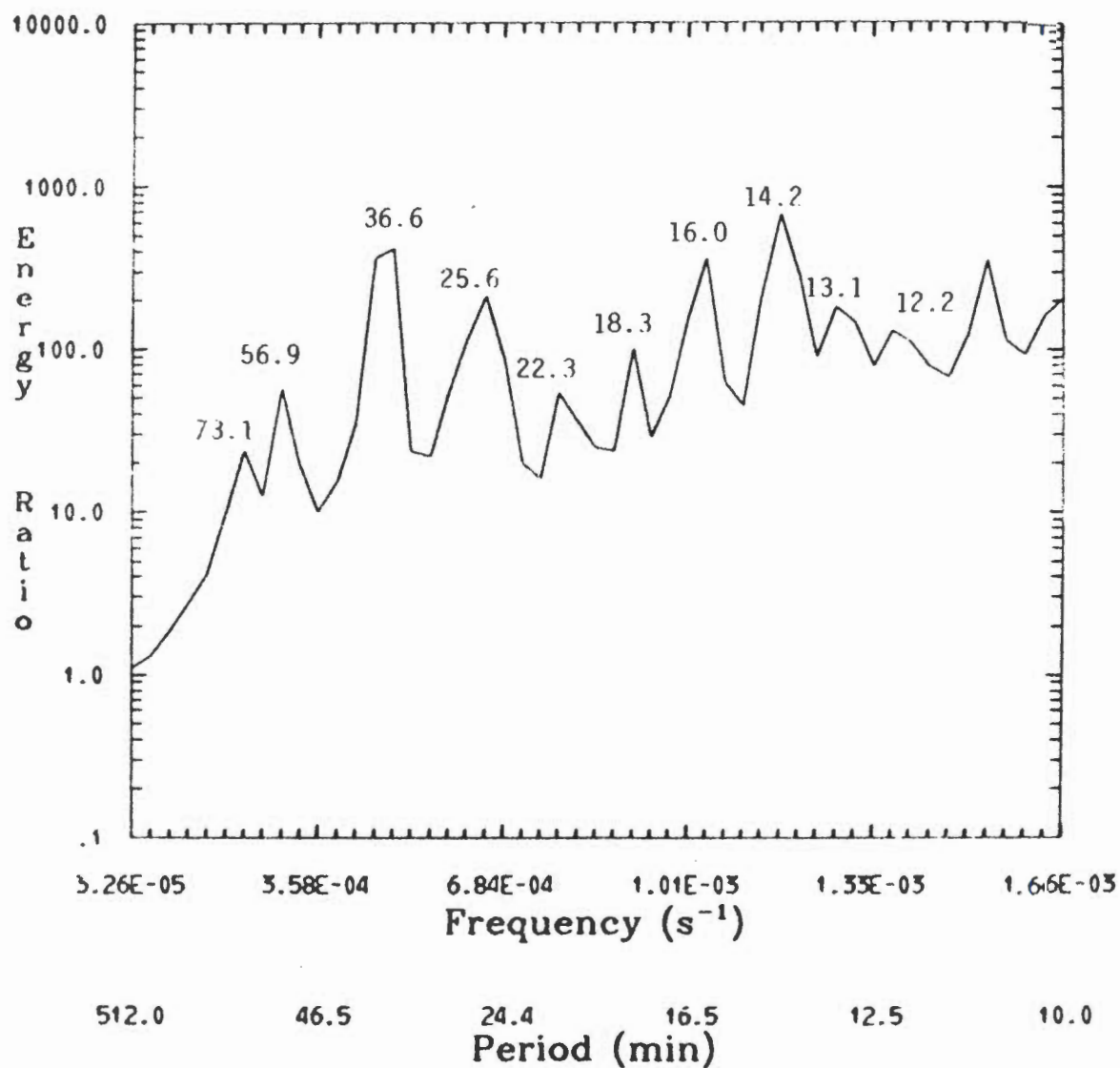


FIG. 4.11. As in Fig. 4.5 except around Maui.

# Hawaii Average - Alaska

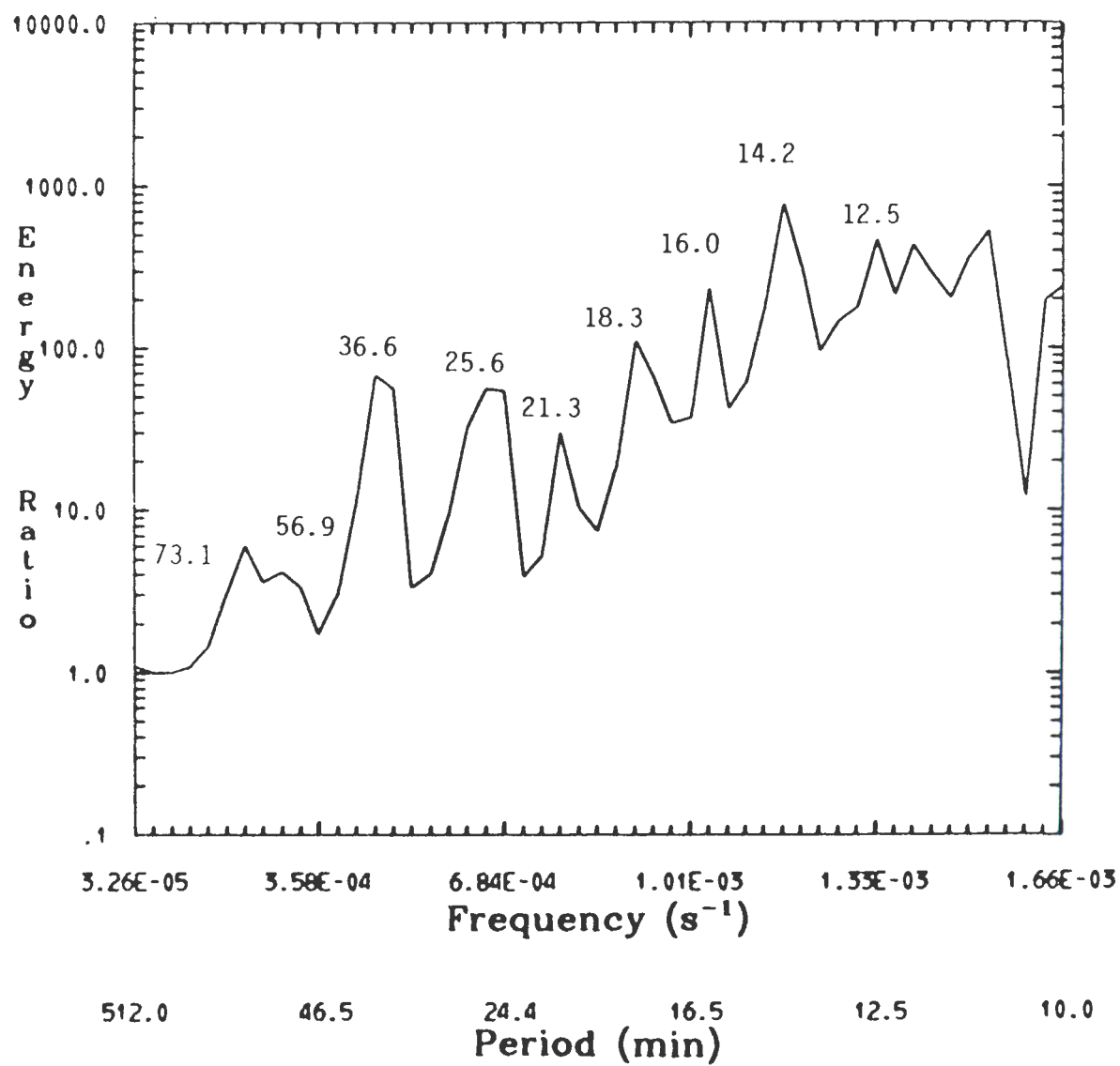


FIG. 4.12. As in Fig. 4.5 except around Hawaii.

TABLE 4.1. Values of averaged energy ratio peaks from individual islands

| Islands   | Period (min) |      |      |      |      |      |      |      |      |      | Additional peaks<br>(period/energy ratio)                         |
|-----------|--------------|------|------|------|------|------|------|------|------|------|---|
|           | 73.1         | 56.9 | 36.6 | 25.6 | 20.5 | 18.3 | 17.7 | 16.0 | 14.2 | 12.5 |   |
| Niihau    | 3            | 5    | 42   | 88   | 99   | 19   | 14   | 309  | 80   | 14   | (23.3/192):(15.5/671):<br>(13.1/159)                              |
| Kauai     | 4            | 3    | 11   | 21   | 779  | 989  | 1999 | 24   | 173  | 13   | (37.4/25):(15.5/73)   |
| Oahu      | 9            | 7    | 65   | 34   | 120  | 106  | 41   | 319  | 70   | 25   | (51.2/11):(24.4/53):(21.3/129):<br>(17.1/112):(14.6/89):(13.5/96) |
| Molokai   | 12           | 41   | 199  | 110  | 64   | 294  | 15   | 373  | 326  | 64   | (13.5/305)  |
| Lanai     | 5            | 36   | 445  | 155  | 19   | 89   | 25   | 258  | 926  | 34   | (21.3/29)   |
| Kahoolawe | 29           | 84   | 333  | 226  | 14   | 35   | 24   | 197  | 1364 | 102  | (34.1/425):(15.5/240):(13.1/191)                                  |
| Mauai     | 24           | 57   | 369  | 216  | 37   | 105  | 31   | 371  | 702  | 93   | (34.1/240):(21.3/55):(13.1/188)                                   |
| Hawaii    | 6            | 4    | 68   | 56   | 10   | 110  | 66   | 230  | 773  | 458  | (21.3/30)   |
| Average   | 10           | 21   | 149  | 91   | 124  | 214  | 157  | 254  | 527  | 184  |   |

| Additional resonant peak associations |                         |              |
|---------------------------------------|-------------------------|--------------|
| Period (min)                          | Island association      | Period (min) |
| 51.2                                  | Oahu                    | 17.1         |
| 37.4                                  | Kauai                   | 15.5         |
| 34.1                                  | Kahoolawe-Mauai         | 14.6         |
| 24.4                                  | Oahu                    | 13.5         |
| 23.3                                  | Niihau                  | 13.1         |
| 21.3                                  | Oahu-Lanai-Mauai-Hawaii |              |
|                                       | Oahu                    |              |
|                                       | Niihau-Kauai-Kahoolawe  |              |
|                                       | Oahu                    |              |
|                                       | Oahu-Molokai            |              |
|                                       | Niihau-Kahoolawe-Mauai  |              |

To determine the response behavior for each shoreline point of individual islands, contours of  $\sqrt{\text{energy ratio}}$  were plotted on a frequency versus perimeter diagram. The  $\sqrt{\text{energy ratio}}$  was contoured for graphical clarity and represents the shoreline amplitude in response to a unit amplitude deep water input. The contour maps are illustrated in Figs. 4.13 through 4.20 with the key for the grid points around the island shown in Figs. 4.21 and 4.22. For each island the perimeter is numbered clockwise starting with the southernmost grid point. The numbering system places the northern part (incident side) of each island in the center of the contour map.

As an aid in the interpretation of the response patterns, travel times between islands and around islands at selected depths were calculated and compiled in Table 4.2. Travel times were based on the propagation speed of long waves in the model system. Table 4.2 also indicates the grid points facing each other on individual islands. For example, grid numbers 8 through 13 on Niihau face grid numbers 3 through 11 on Kauai, disclosing that resonances between Niihau and Kauai may be found at a period of 14.7 minutes on the contour maps. Examination of Fig. 4.13 and Fig. 4.14 reveals peaks in response amplitude in the areas facing each island. Travel times were computed around each island (or island group) at depths of 500, 1000, and 2000 meters. It should be understood that these travel times are only roughly indicative of those corresponding to true wave rays. The trapped wave rays will follow the path of least time whether it be on a contour or not. Further, local resonances coupled with trapped waves and interinsular reflections may combine to reinforce or

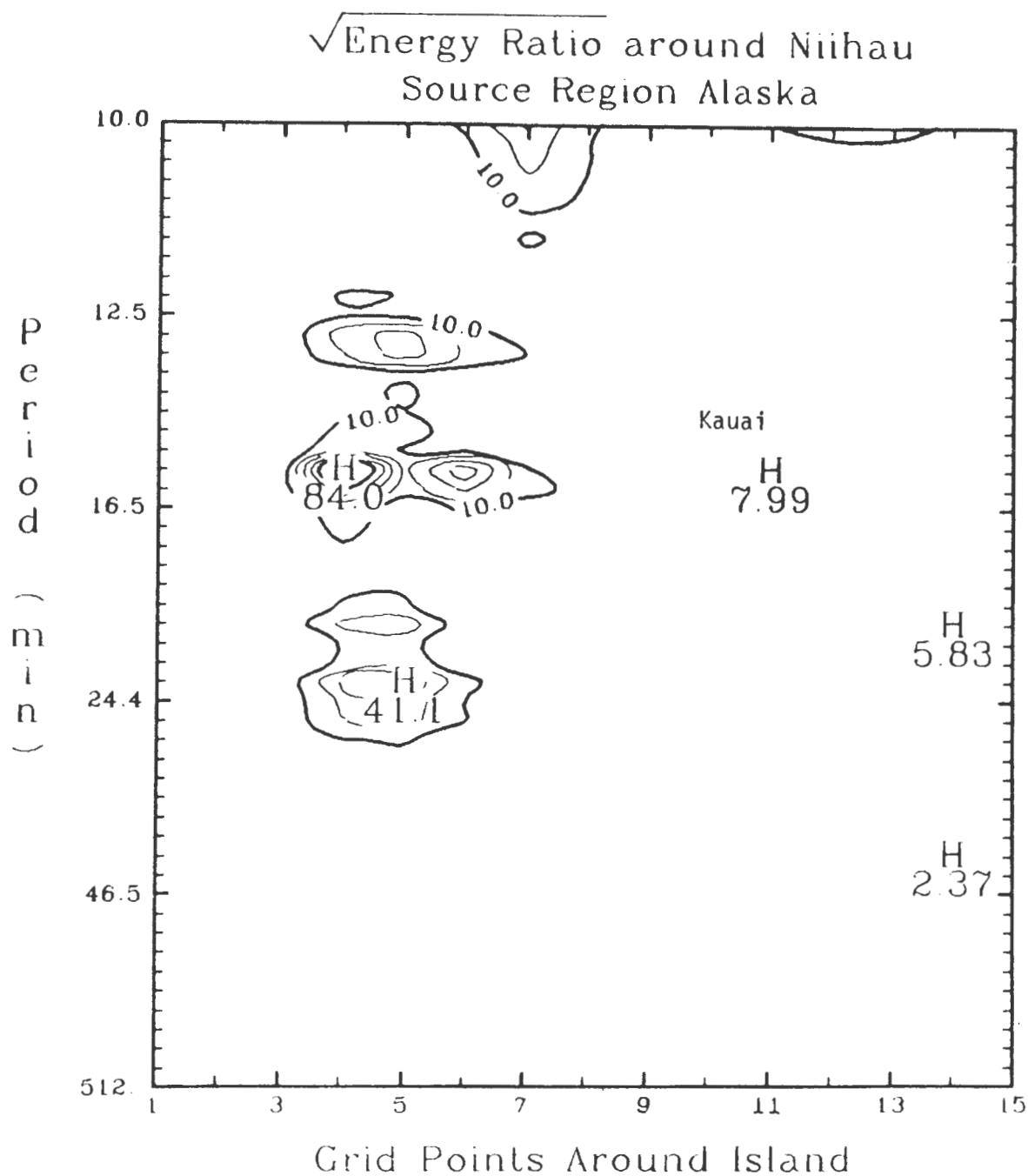


FIG. 4.13. Contour of  $\sqrt{\text{energy ratio}}$  around Niihau. The heavy contours are 10.0, 50.0, and 150.0; the light contours are 20.0, 30.0, 40.0, 100.0, and 200.0. H indicates peak value and the grid points are keyed to Fig. 4.21 and 4.22.

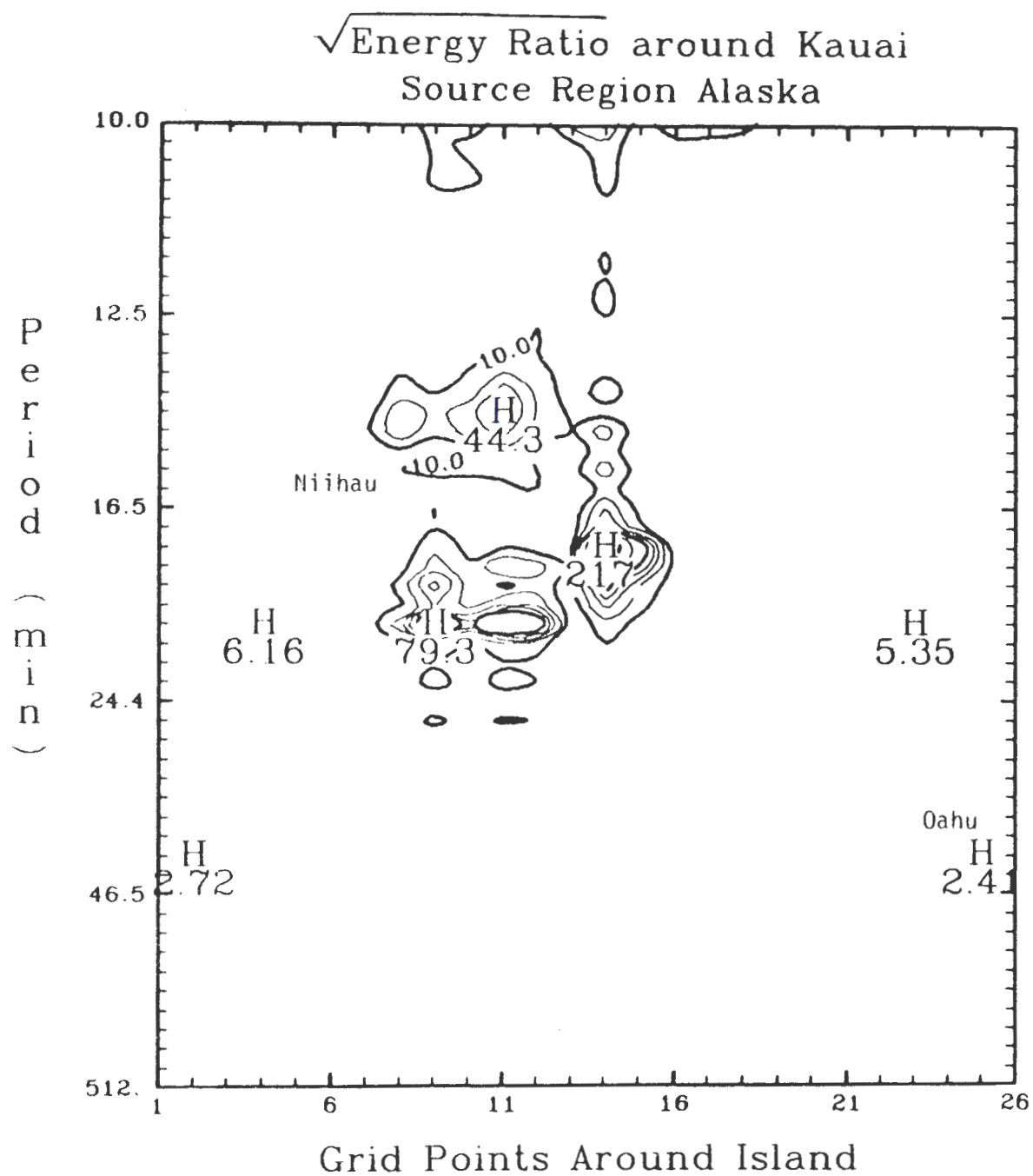


FIG. 4.14. As in Fig. 4.13 except for Kauai.





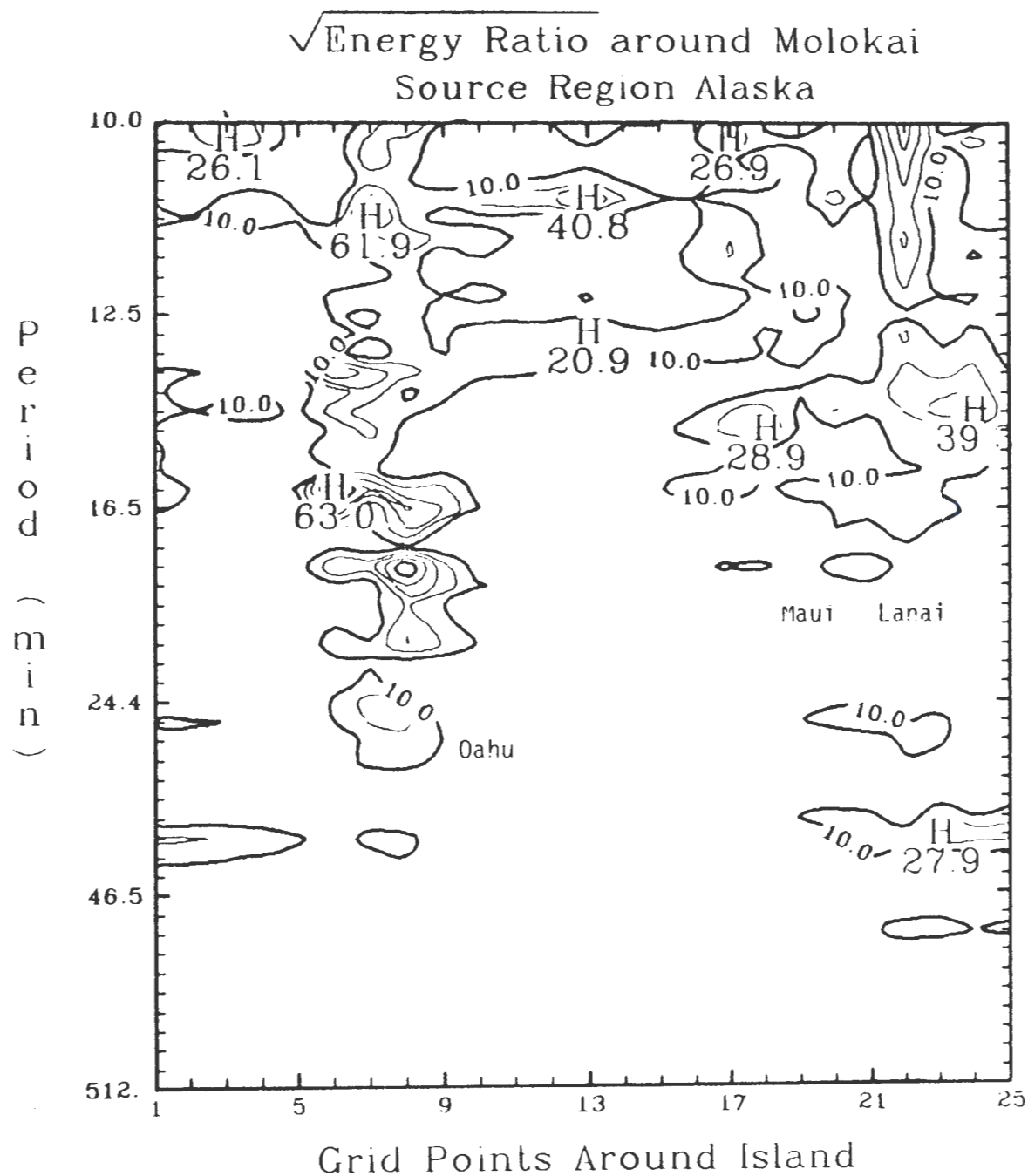


FIG. 4.16. As in Fig. 4.13 except for Molokai.

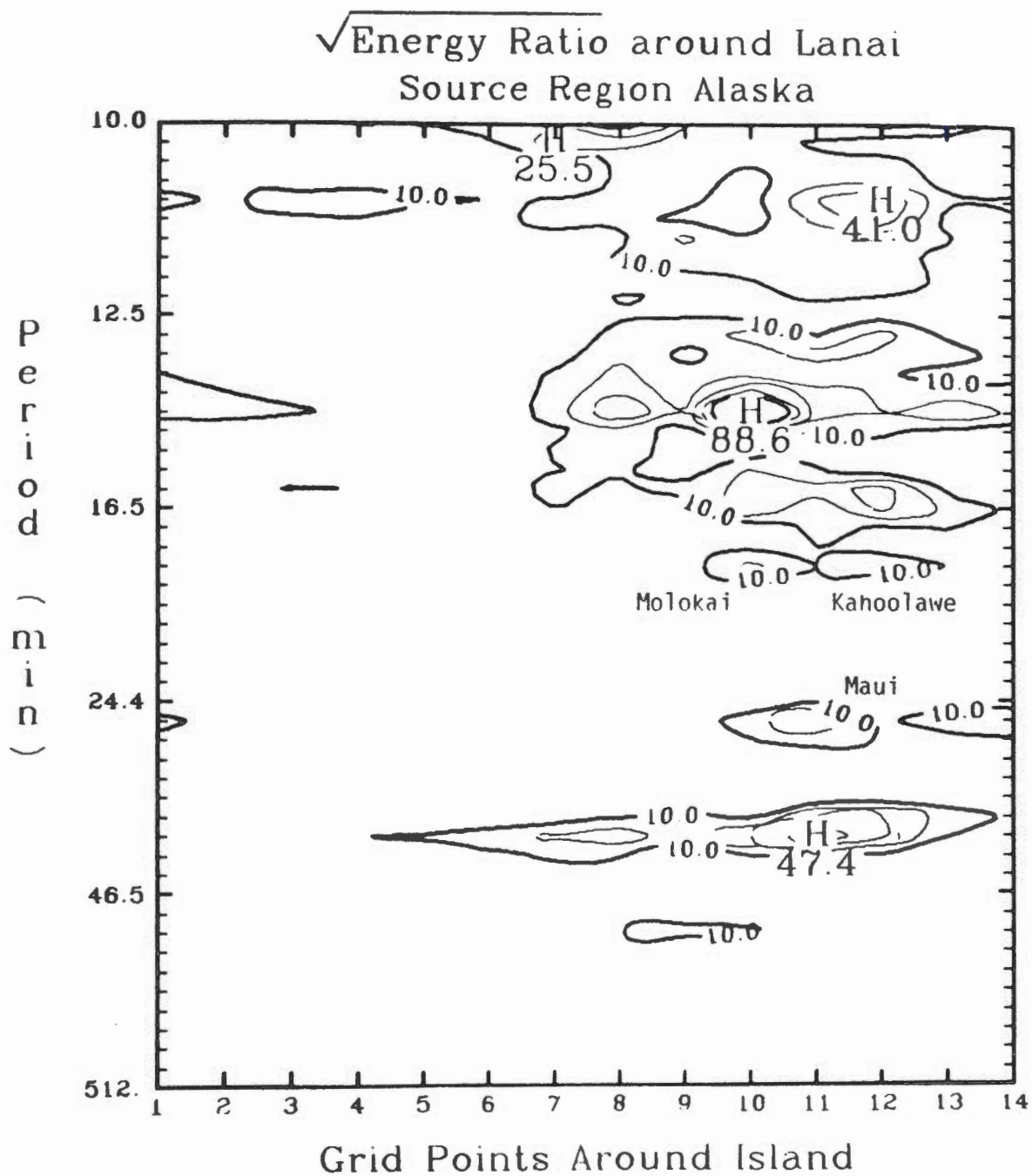


FIG. 4.17. As in Fig. 4.13 except for Lanai.

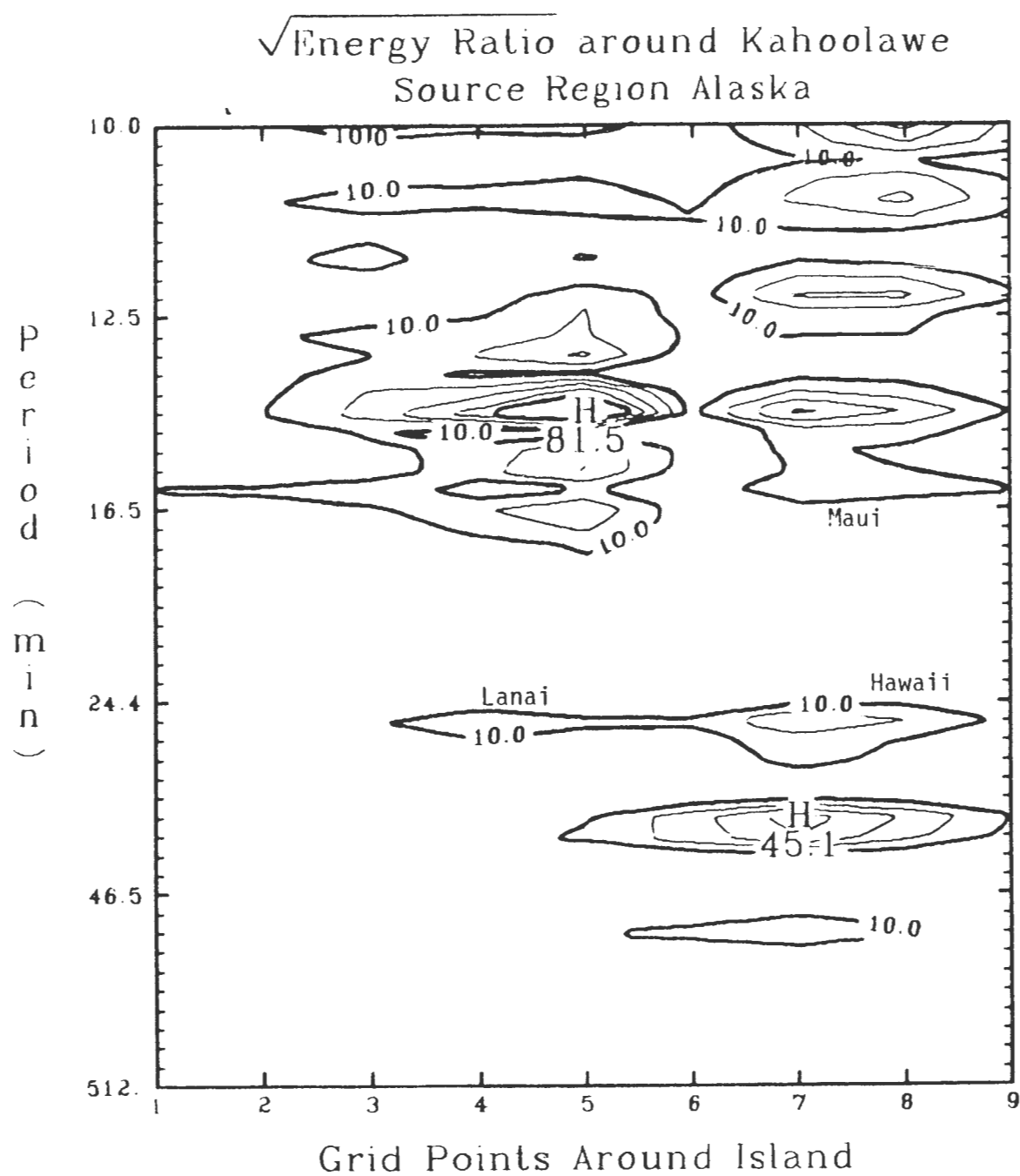


FIG. 4.18. As in Fig. 4.13 except for Kahoolawe.

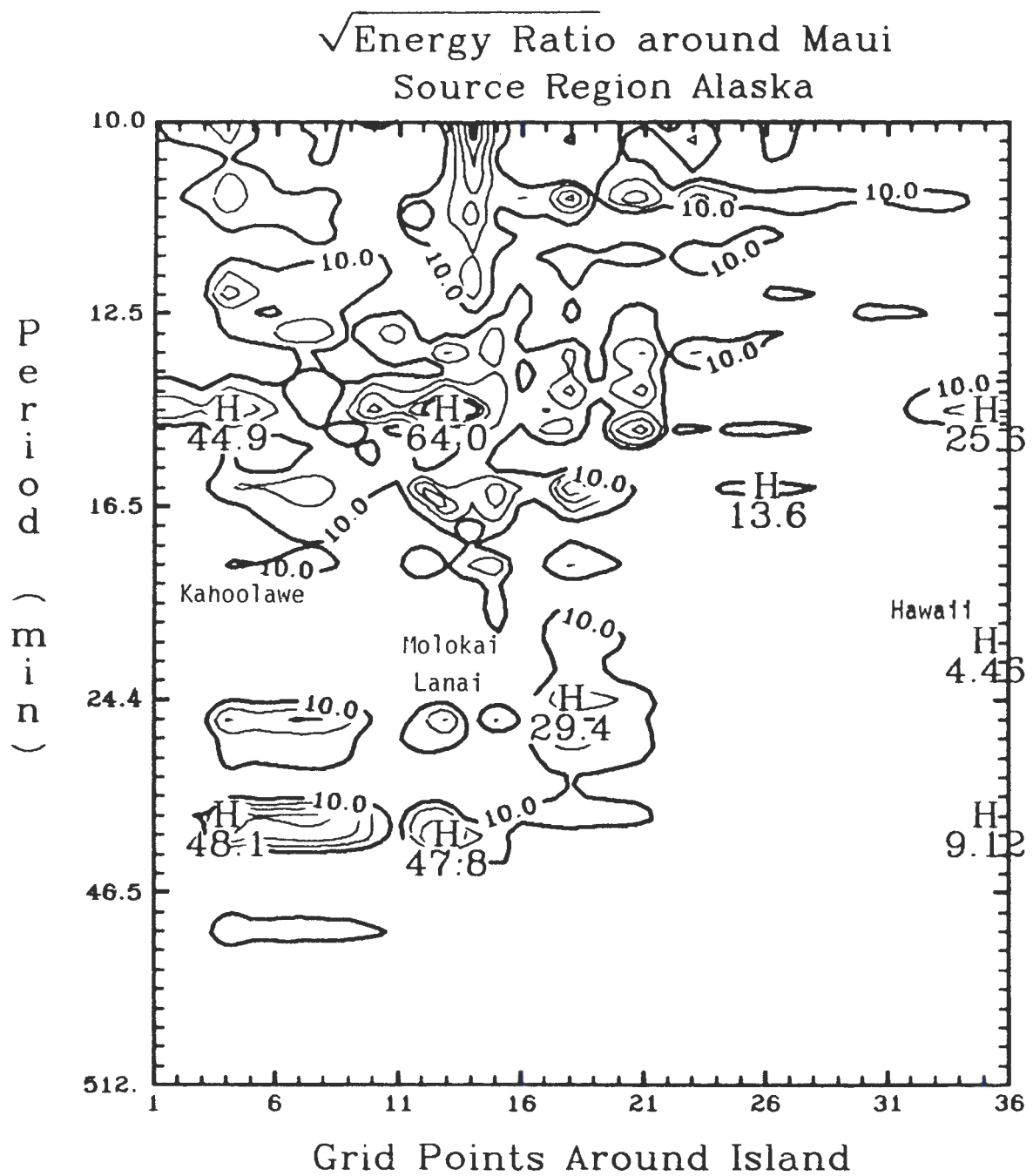


FIG. 4.19. As in Fig. 4.13 except for Maui.

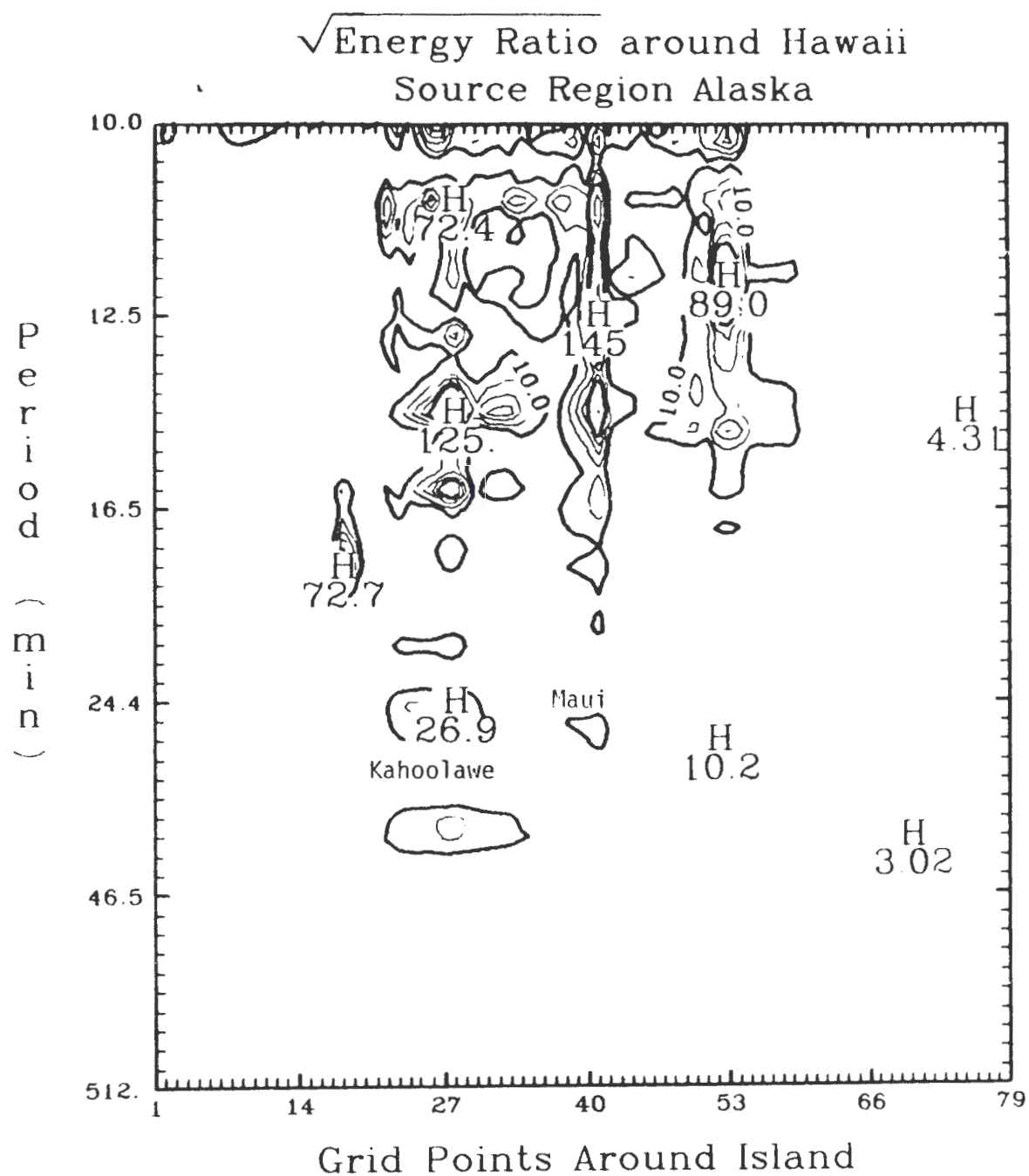


FIG. 4.20. As in Fig. 4.13 except for Hawaii.

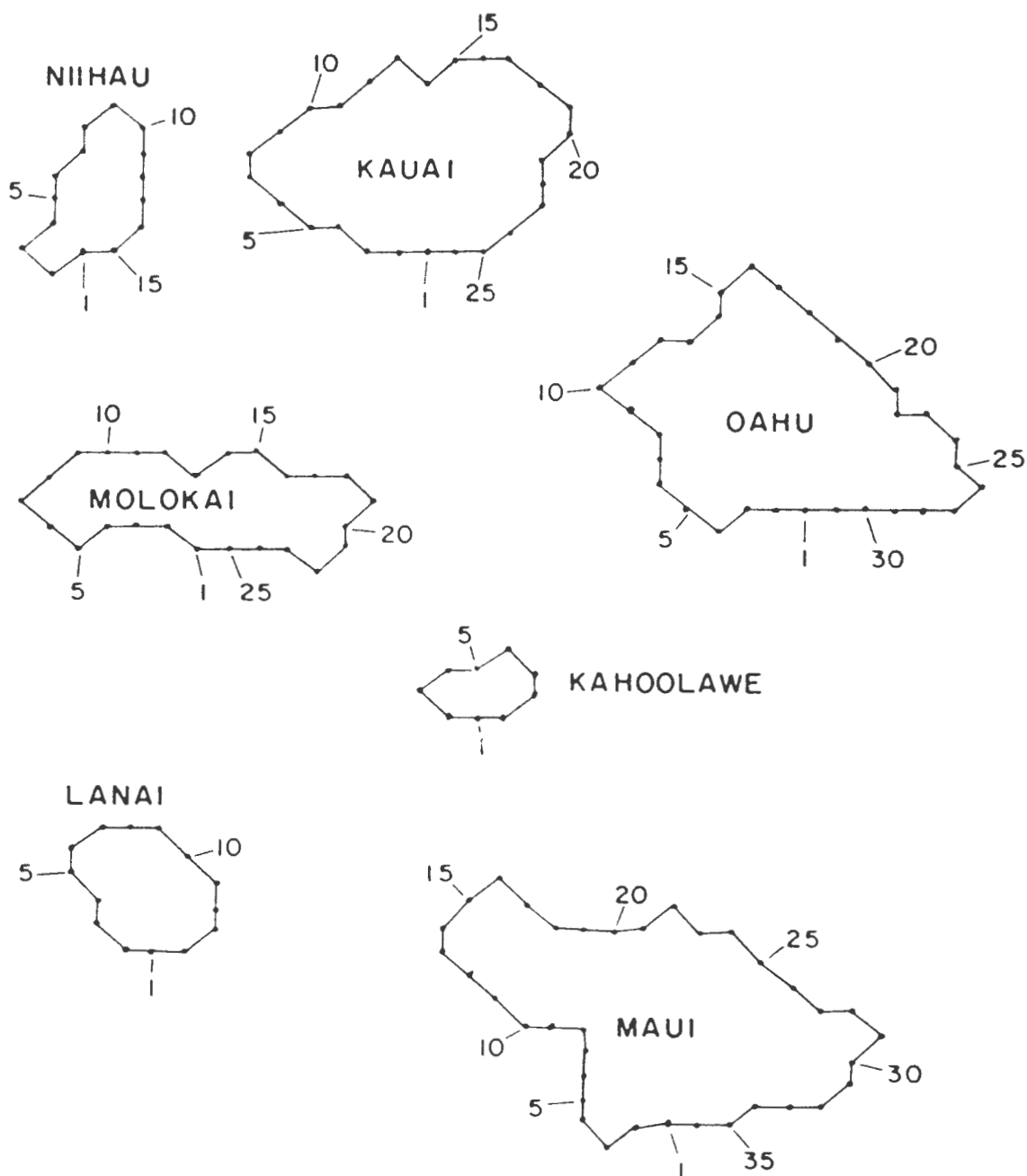


FIG. 4.21. Key for grid points around island for seven model Hawaiian Islands.

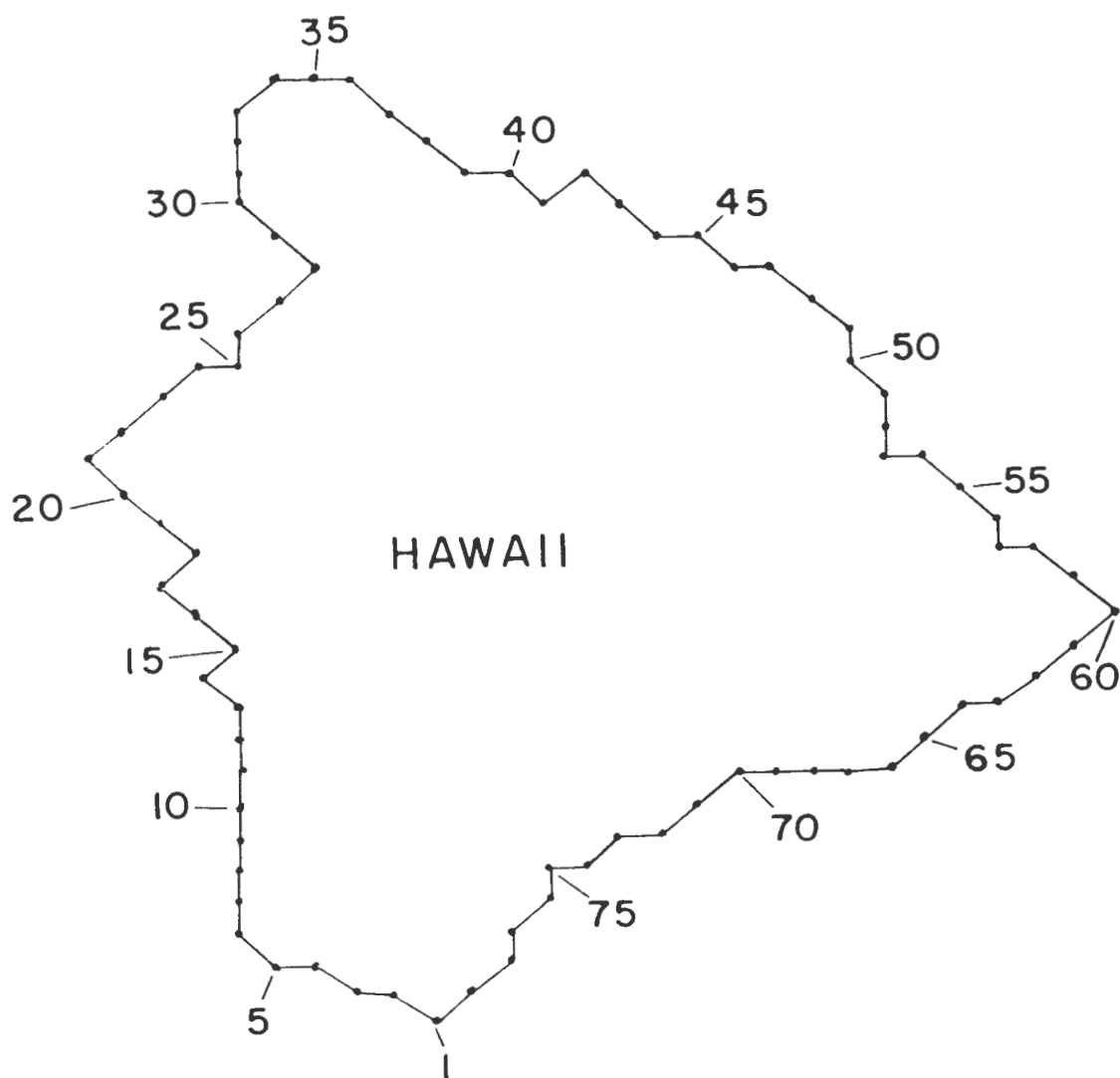


FIG. 4.22. Key for grid points around the model island of Hawaii.

TABLE 4.2. Travel times between islands and around islands at selected depths

| Island combination | Travel time (min) | Opposite grid points |       |         |       |
|--------------------|-------------------|----------------------|-------|---------|-------|
| Niihau-Kauai       | 14.7              | Niihau               | 8-13  | Kauai   | 3-11  |
| Kauai-Oahu         | 40.0              | Kauai                | 19-25 | Oahu    | 5-16  |
| Oahu-Molokai       | 29.6              | Oahu                 | 24-29 | Molokai | 5- 9  |
| Molokai-Lanai      | 19.9              | Molokai              | 23- 3 | Lanai   | 6-11  |
| Molokai-Maui       | 23.7              | Molokai              | 19-22 | Maui    | 11-15 |
| Lanai-Maui         | 26.4              | Lanai                | 11-13 | Maui    | 9-13  |
| Kahoolawe-Lanai    | 22.7              | Kahoolawe            | 3- 7  | Lanai   | 12- 1 |
| Kahoolawe-Maui     | 16.8              | Kahoolawe            | 6- 8  | Maui    | 3- 7  |
| Maui-Hawaii        | 25.9              | Maui                 | 31-35 | Hawaii  | 33-37 |
| Kahoolawe-Hawaii   | 27.9              | Kahoolawe            | 8- 1  | Hawaii  | 23-28 |

Travel times around islands at selected depths

| Depth (m) | Island                            | Travel time (min) |
|-----------|-----------------------------------|-------------------|
| 500       | Niihau                            | 21.7              |
| 500       | Kauai                             | 45.2              |
| 500       | Oahu                              | 65.8              |
| 500       | Oahu-Molokai-Lanai-Maui-Kahoolawe | 129.0             |
| 500       | Hawaii                            | 116.3             |
| 1000      | Kauai-Niihau                      | 65.8              |
| 1000      | Oahu-Molokai-Lanai-Maui-Kahoolawe | 143.0             |
| 1000      | Hawaii                            | 95.4              |
| 2000      | Kauai-Niihau                      | 54.6              |
| 2000      | Oahu-Molokai-Lanai-Maui-Kahoolawe | 116.0             |
| 2000      | Hawaii                            | 83.8              |



diminish excited modes, allowing an indeterminate number of resonant combinations. The travel times in Table 4.2 are given only to suggest simple resonant associations.

With the aid of Tables 4.1 (page 54), 4.2 (page 66), and Figs. 4.13 (page 56) through 4.20, some interpretation of the response of a tsunami approaching the Hawaiian Islands from Alaska can be made. Starting with Niihau (Fig. 4.13, page 56), a peak is seen opposite Kauai at approximately 15.0 minutes, and another peak is seen at grid points 3 through 5 at 21.7 minutes. The 21.7-minute period coincides with the travel time around Niihau at the 500-m contour (Table 4.2, page 66). The other peak at 16.5 minutes and 12.8 minutes may be caused by resonances created by the local bathymetry.

For Kauai in Fig. 4.14 (page 57), the 14.7-minute peak appears opposite Niihau and a 40.0-minute peak appears opposite Oahu. The 45.2-minute peak at grid points 1 and 26 can be associated with the travel time around Kauai at 500 m (Table 4.2, page 66). The enormous peak at 17.7-minute period at point 14 is related geographically to Hanalei Bay where historically high amplitudes have been observed (Pararas-Carayannis, 1969).

The Oahu contour map (Fig. 4.15, page 58) does not show either the Kauai-Oahu reflection or the Oahu-Molokai reflection. These two reflections were the only interinsular travel times for the eight Hawaiian Islands that did not have a counterpart on the contour maps. For this reason, the Oahu average response (Fig. 4.7, page 48) was inspected. A rise corresponding to the Oahu-Kauai travel time (40.0 minutes) was found at 39.4 minutes. The apparent contradiction was

solved by examining the individual transfer functions on Oahu at grid points 5 through 16. The transfer functions showed a peak at 39.4 minutes, with values ranging from 1.5 to 10.5. Because the contour program's lowest level was 10.0, a contour was not drawn for the two values greater than 10.0. This points out a problem that can arise by using only the contour maps. By using the contour maps with the averaged response, many additional features can be resolved. In addition to the 39.4-minute peak in Fig. 4.7 (page 48), a peak is observed at 73.1 minutes corresponding to the Oahu 500-m contour travel time (65.8 minutes).

The Molokai, Lanai, Kahoolawe, Maui island group contributes the most resonant energy to the nine peaks in Fig. 4.4 (page 45). The complicated response patterns are created because of the nearness of the islands to each other and shallowness of the water between them. By looking at the energy ratio versus frequency graphs of Fig. 4.9 (page 50) and 4.10 (page 51), the island average of Lanai and Kahoolawe, it is revealed that a resonant peak exists between 170.6 and 128.0 minutes. Corresponding to this period range is the 1000-m contour around the complex with a travel time of 143.0 minutes. The travel time between island resonance is evident on each island contour (Figs. 4.16, page 59, through 4.19): Molokai-Lanai, 19.9 minutes; Molokai-Maui, 23.7 minutes; Lanai-Maui, 26.4 minutes; Kahoolawe-Lanai, 22.7 minutes; Kahoolawe-Maui, 16.8 minutes. Each island shows a minor resonant peak at locations opposite other islands and at the appropriate period associated with respective islands (Table 4.2, page 66). Molokai (Fig. 4.16, page 59) also shows the reflection resonance of

Oahu at 29.6 minutes. The Maui and Kahoolawe contours (Figs. 4.19, page 62, and 4.18) display the reflection off Hawaii at 25.9 minutes and 27.9 minutes, respectively.

The largest island, Hawaii, has suffered the most tsunami damage at Hilo. In the model, Hilo is represented by grid point 53 on the Hawaii contour (Fig. 4.20, page 63). Around this point a high ridge in the response amplitude appears at periods higher than 16.5 minutes. During the April 1, 1946 tsunami, 173 people were killed, 163 injured, 488 buildings demolished, 936 damaged, the waterfront washed out, and the tide gauge destroyed (Pararas-Carayannis, 1969) at Hilo. Shepard *et al.* (1950) reported that for that tsunami the principal period observed was between 14 and 15 minutes which corresponds well with the high energy peak of Fig. 4.20. The reflection resonances off Kahoolawe and Maui are visible at periods of 27.9 and 25.9 minutes. No peaks have been associated with the travel times around Hawaii.

The complexity of the Hawaiian Islands' response to tsunamis cannot be overstated. The case for a tsunami originating in Alaska has been shown in averaged and contoured form to examine the gross and detailed features of the response patterns. Certain characteristics of the whole system as well as individual islands may be correlated with simple travel times between and around islands, but the resolution of a complete interpretation will require an extensive numerical and analytic effort.

## CHAPTER V

## SUMMARY AND RECOMMENDATIONS

5.1 Summary of Results

A numerical modeling procedure has been developed and verified to simulate the response of islands to sharp pulses. Peaks in the response patterns identify wave periods trapped by the bathymetry that create higher amplitude shoreline water elevations. The modeling method has been applied to the eight major Hawaiian Islands, resulting in response patterns for each shoreline grid point. Appraisal of the response patterns of the Hawaiian Islands model has led to the following conclusions:

1. The few historical observations available for comparison indicate the model accurately determines areas of tsunami susceptibility for the State of Hawaii.
2. Based upon a system averaged response, the model indicates the Hawaiian Islands are most responsive to tsunamis originating around Alaska which are energetic in periods of 14.2, 18.3, 16.0, 12.5, 36.6, 20.5, 25.6, 56.9, and 73.1 minutes, respectively.
3. Based upon travel time comparisons, the model indicates that reflections between islands establish resonances which contribute to or constitute peaks in the response patterns.
4. The model indicates that the energy concentration experienced at Hilo, Hawaii during the 1946 tsunami was partly due to the response of the island bathymetry to the 14-15 minute period tsunami.

## 5.2 Future Research

Two immediate applications of the Hawaiian Islands model should be (1) to evaluate the response patterns for a set of different approach angles and (2) to use the output as input for a more detailed nearshore model. An investigation to determine the tsunami susceptibility of the State of Hawaii as a function of approach angle would aid in establishing insurance and coastal planning criteria. The second application of the Hawaiian model would be as a source of input data for more detailed numerical models. Since the time history of the water elevation is recorded at each grid point, the present model could provide input time sequences along the borders of the area of interest. In this manner, the more detailed model would represent the action of the island system without modeling the whole system. The simulation efforts could include the remote reflection effect at a fraction of the computer expenditure.

The present model has been tested for cases where the incident wave approaches the islands at an angle with respect to the grid configuration. The results indicate that the open boundary rendition is inadequate to properly model this simulation. More refined numerical techniques must be combined with the present model to undertake the study of response patterns produced by different approach angles.

## REFERENCES

- Bernard, Eddie N., 1973: Bathymetric representation for computer models. Rept. No. 90, Joint Tsunami Research Effort, Hawaii Institute of Geophysics, University of Hawaii.
- Brandsma, M., D. Divoky and L-S. Hwang, 1974: Response of small islands to long waves. Tetra Tech, Inc., Tech. Rept. NVD-289-12.
- Cochrane, J. D., and R. S. Arthur, 1948: Reflection of tsunamis. *J. Marine Res.*, 7, 239-251.
- Homma, S., 1950: On the behaviour of seismic sea waves around a circular island, *Geophys. Mag.*, 21, 199-208.
- Jordaan, Jan Malan, Jr., and William M. Adams, 1968: Tsunami height, Oahu, Hawaii: Model and nature. *Proc. of the 11th Conference on Coastal Engineering*, 1, 1555-1574.
- Knowles, Charles E., and Robert O. Reid, 1970: The inverse tsunami problem for symmetric islands of simple shape. Reference 70-7T, Dept. of Oceanogr., Texas A&M University, 69 pp.
- Longuet-Higgins, M. S., 1967: On the trapping of wave energy round islands. *J. Fluid Mech.*, 29, 781-821.
- Loomis, Harold G., 1972: A package program for time-stepping long waves into coastal regions with application to Haleiwa Harbor, Oahu. Rept. No. HIG-72-21, Hawaii Institute of Geophysics, University of Hawaii.
- Muirhead, C. R., 1967: Investigation of possible resonant excitation at an island by tsunamis. M.S. thesis, Texas A&M University, 36 pp.
- Omer, Guy C., Jr., and H. H. Hall, 1949: The scattering of tsunamis by a cylindrical island. *Bull. Seis. Soc. Amer.*, 39, 257-260.
- Pararas-Carayannis, George, 1969: Catalog of tsunamis in the Hawaiian Islands. Rept. No. 69-2, World Data Center A.
- Platzman, George W., 1958: A numerical computation of the surge of 26 June 1954 on Lake Michigan, *Geophysica*, 6, 407-438.
- Reid, R. O., and B. R. Bodine, 1968: Numerical model for storm surges in Galveston Bay. *J. Waterways and Harbors Div. Proc. ASCE*, 94, 33-57.

- Roache, Patrick J., 1972: *Computational Fluid Dynamics*. Hermosa Publ., Albuquerque, N. M., 434 pp.
- Shapiro, M. A., and J. J. O'Brien, 1970: Boundary conditions for fine-mesh limited-area forecasts. *J. Appl. Meteor.*, 9, 345-349.
- Shepard, F. P., G. A. MacDonald and D. C. Cox, 1950: The tsunami of April 1, 1946. *Bull. Scripps Inst. Oceanogr.*, 5, 391-528.
- Taylor, J., P. Richards, and R. Halstead, 1971: Computer routines for surface generation and display. M.S. Rept. Ser. No. 16, Dept. Energy, Mines & Resources, Ottawa.
- Vastano, A. C., and E. N. Bernard, 1973: Transient long-wave response for a multiple island system. *J. Phys. Oceanogr.*, 3, 406-418.
- \_\_\_\_\_, and R. O. Reid, 1966: A numerical study of the tsunami response at an island. Reference 66-26T, Dept. of Oceanogr., Texas A&M University, 141 pp.
- \_\_\_\_\_, and R. O. Reid, 1970: Tsunami response at Wake Island: Comparison of hydraulic and numerical approaches. *J. Marine Res.*, 28, 345-356.